Geometrically Nonlinear Coupled Adjoint Aerostructural Optimization of Natural-Laminar-Flow Strut-Braced Wing

Yiyuan Ma[1], and Morteza Abouhamzeh[2]
Technische Universität Braunschweig, Braunschweig, 38108, Germany
and
Ali Elham[3]
University of Southampton, Southampton SO16 7QF, United Kingdom

Novel aircraft concepts employing ultra-high aspect ratio wings, such as the Strut-Braced Wing (SBW) configuration, are promising ways to achieve the next-generation sustainable and fuel-efficient aviation goals. However, as the wing aspect ratio increases, the wing increasingly exhibits more flexibility, higher deformation, and geometrically nonlinear behavior that cannot be accurately simulated by conventional sizing methods and typical linear structural analysis models. This paper establishes a framework for SBW aircraft conceptual design, conceptual optimization, and aerostructural optimization. The presented aerostructural optimization method has medium-fidelity and physics-based features. A geometrically nonlinear structural analysis solver and a quasi-three-dimensional aerodynamic solver are coupled for the aerostructural optimization of composite, natural-laminar-flow SBW aircraft. A medium-range (MR) SBW aircraft is initially designed and optimized in the conceptual design stage. A gradient-based aerostructural optimization is performed using the proposed tool for minimizing the fuel mass of the initially sized and optimized MR-SBW aircraft. The optimization results in a more than 10% reduction in fuel

[1] PhD Student, Institute of Aircraft Design and Lightweight Structures, yiyuan.ma@tu-braunschweig.de
[2] Postdoctoral Researcher, Institute of Aircraft Design and Lightweight Structures
[3] Professor, Computational Engineering and Design Group

mass, more than 8% reduction in aircraft MTOM, and more than 30% reduction in wing and strut structural weight by optimizing the wing box structure, wing planform, and airfoils shape while satisfying the constraints on structural failure, wing loading, and aileron effectiveness.

Nomenclature

AR	=	aspect ratio
C_l	=	lift coefficient
G	=	parameters for Chebyshev polynomials
G_{st}	=	strut airfoil's scaling factor
k	=	fraction
L_δ	=	roll moment due to an aileron deflection, N.m
m	=	mass, kg
M_a	=	Mach number
M_{ff}	=	fuel mass fraction
MTOM	=	maximum takeoff mass, kg
n	=	load factor
OEM	=	operating empty mass, kg
P	=	wing planform vector
Q	=	transformed and reduced material coefficient of the composite material
U	=	nodal displacement matrix
W	=	weight, N
X	=	design variables vector
α	=	angle of attack, deg

α_i = incidence angle state variable, deg

Γ = vortex rings strengths

η_α = aileron effectiveness

η_{st} = normalized spanwise strut attachment position

Λ = sweep angle, deg

λ = taper ratio

φ = coupled adjoint vector

Subscripts

AIC = aerodynamic influence coefficient

F = Fuel

R = reserve fuel

RHS = right hand side

S = strut

W = wing

W+S = wing and strut

I. Introduction

Air transportation has been growing rapidly in most regions of the world and is predicted to continue to grow in the coming decades. Boeing and Airbus both forecast in their Commercial Market Outlook [1] and Global Market Forecast [2] that the revenue passenger kilometer will continue to grow by over 4% annually. However, aviation also contributes a significant amount of greenhouse gases and other pollutants, including nitrogen oxide, sulfur dioxide, and noise. In total, air transportation is responsible

for 1-2% of global human-made CO_2 emissions [3]. NASA and the European Commission have proposed ambitious sustainable aviation goals to mitigate the environmental impact of the continued growth in air traffic volume [4, 5]. Grewe et al. [6] presented that although the emissions targets for aviation are in line with the overall goals of the Paris Agreement, aviation's impact on climate is likely to fall short of these goals. Therefore, the integration of novel airframe and energy network technologies is necessary and urgent for the aviation industry.

The Ultra-High Aspect Ratio Wing (UHARW) configuration is one of the promising concepts to achieve sustainable aviation goals through improving aerodynamic efficiency. Whereas the lower induced drag of the UHARW configuration improves aircraft fuel efficiency, the aerodynamic load-caused wing bending moment and shear force in the UHARW structure are significant, resulting in increased wing structural weight and limiting the overall benefits. For example, for medium-range transport aircraft with conventional cantilever wings, the mission fuel mass increases exponentially with the increase in wing aspect ratio when the aspect ratio exceeds 16 [7]. To address this issue, on the one hand, the Strut-Braced Wing (SBW) configuration can be employed to mitigate significant loads in UHARW structures [8], and on the other hand, advanced composite materials such as Carbon Fiber Reinforced Polymers (CFRP) can be applied in UHARW structures to reduce the wing structural weight [9].

SBW aircraft utilize additional structural elements, struts, to connect the main wing to the fuselage to stiffen the wing structure. The wing bending moment can thus be reduced by significant amounts, allowing for reduced wing thickness-to-chord ratio and chord [10]. The reduction in wing thickness results in decreased wing wave drag, which allows for a lower wing sweep angle, thereby reducing wing spanwise crossflow disturbances [11]. The combined effects of reduced spanwise crossflow and

decreased Reynolds number lead to an increased extent of wing laminar flow. Due to these advantages, the SBW concept has been studied extensively. The SUGAR project conducted a comprehensive study of the SBW configuration for the next generation of Medium-Range (MR) missions [12]. Virginia Polytechnic and State University performed conceptual design and optimization research for a long-range SBW aircraft [13]. Carrier et al. [14] are researching an overall aircraft conceptual design framework for SBW aircraft that combines high-fidelity aerodynamic and structural analysis. NASA is funding research on aerodynamic optimization and aeroelastic analysis for SBW aircraft [15, 16]. Although there are studies on SBW aircraft's aerodynamic optimization [8, 16, 17] and Multidisciplinary Design Optimization (MDO) [13, 18, 19], there is a need for the mid-fidelity wing aerostructural analysis and optimization method of SBW aircraft that computes the wing drag and structural deformation with a level of accuracy comparable to the higher fidelity methods in early design stages, where the wing structure data are not sufficient for high-fidelity analysis and optimization.

UHARW are naturally more flexible than conventional wings and exhibit larger deformation. This is especially true when they are made of composites, which have higher failure strains than metallic materials [20]. Due to their high flexibility, UHARW have geometrically nonlinear behaviors, which cannot be accurately modeled using linear structural analysis methods. Due to the inaccurate calculation of the linear stress and the inaccurate deflection of the wing shape, the use of linear models may lead to inaccurate sizing of the wing structure, which can influence the aerodynamic load distribution on the wing [21]. Geometrically nonlinear structural analysis methods are available in many structural analysis codes and have been incorporated into some aeroelastic analysis tools [22, 23]. Werter and De Breuker developed a geometrically nonlinear beam model for dynamic aeroelastic analysis of aircraft wings and studied the benefits of aeroelastic tailoring in wing weight reduction [24]. Conlan−Smith and Andreasen

coupled a nonlinear finite element model and a three-dimensional panel method for static shape optimization of aircraft wings with large deformations [25]. Gray and Martins developed a high-fidelity geometrically nonlinear aerostructural optimization method for high aspect ratio wings [21]. Achard et al. [26] developed and investigated two different methods for high-fidelity aerostructural gradients computation, and applied these methods to the aerostructural optimization research of the ONERA M6 and Common Research Model wings.

As described above, due to the high flexibility characteristic of UHARW, it is necessary to consider geometric nonlinearities for analysis and optimization. For high aspect ratio SBW, although the strut limits the wing's deformation, the aeroelastic analysis of SBW still needs to consider geometric nonlinearities due to the strut's high deformation and apparent buckling under negative load case, as illustrated in Fig. 1. McDonald et al. [27] reviewed the progress of SBW research and concluded that the primary considerations for future SBW research are nonlinear structural design and nonlinear aeroelastic analysis. Sohst et al. [28] conducted a comparative study of linear and nonlinear models for SBW aeroelastic analysis and pointed out that the consideration of geometric nonlinearities in the SBW aeroelastic optimization is necessary due to the complex geometric behavior of SBW. When geometric nonlinearities in the structural model are taken into account, the structural stiffness becomes dependent on the displacements, and significant deformation differences occur between the linear model and the nonlinear model. They found that the linear model showed only a slight curvature of the strut under a negative load case, but the strut's deformation is remarkably bent when geometric nonlinearities were taken into account (similar to Fig. 1). Besides, their results showed that there is a 2% difference in the lift-to-drag ratio of the optimized SBW obtained using linear and nonlinear models, which has a non-negligible impact on the aircraft performance estimation. Therefore, according to the above-mentioned

previous research results, the geometrically nonlinear model is utilized in this study for the SBW aerostructural optimization.

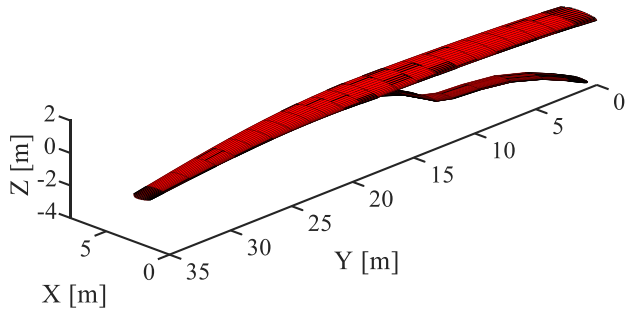

Fig. 1 Wing and strut deformation with geometric nonlinearities under negative load.

Natural Laminar Flow (NLF) is one of the most promising approaches for drag reduction because of the lower skin friction drag, which maintains a large laminar flow range by shaping the airfoil shape and wing platform with a favorable pressure distribution [29]. Xu and Kroo [30] integrated NLF into aircraft conceptual design and investigated the benefits of NLF design by comparing turbulent and NLF aircraft for mid-range transport missions. However, there are challenges/limitations in implementing NLF on the wings of transport aircraft. A large amount of wind tunnel experiments and flight tests concluded that the wing sweep angle should be no larger than 23 deg, the Mach number should be less than 0.75, and the Reynolds number should be less than 25 million to achieve NLF on the wing due to the cross-flow instability [31]. Because of the same consideration, Kruse et al. [32] investigated the potential of utilizing the forward-swept wing concept for an NLF transonic transport aircraft design. Aerodynamic shape optimization and aerostructural optimization of swept NLF wings in the transonic region are still challenging in terms of the reasonable compromise of wave and viscous drags and the

reliable prediction of laminar-turbulence transition [33].

Aileron effectiveness is an important constraint in wing aerostructural design. Elham and van Tooren [34] studied the influence of aileron effectiveness on the wing weight of A320 aircraft and the results showed that the wing weight varies quadratically with the aileron effectiveness. Riso et al. [35] investigated the influence of aileron effectiveness on the roll maneuverability of high aspect ratio wing aircraft. Sanghi et al. [36] studied the effect of aileron placement on the aileron effectiveness of high aspect ratio wing aircraft. However, although there are some studies on aileron design and roll maneuverability analysis for high aspect ratio wings, few studies have considered aileron effectiveness constraints in the aerostructural optimization of UHARW.

Gradient-based optimization methods are more effective than heuristic optimization methods for most aerostructural optimization problems with a large number of design variables [37]. Furthermore, coupled adjoint sensitivity analysis approach calculates derivatives efficiently for the coupled aerostructural optimization problems by solving a linearization of the governing equations [38]. Kennedy et al. [39] utilized the adjoint method for the wing aerostructural optimization of a large transport aircraft. Gray and Martins [21] performed a high-fidelity aerostructural optimization study for highly flexible wings by using the adjoint sensitivity analysis method. Brooks et al. [40] developed a methodology for the aerostructural optimization of tow-steered composite wings using the adjoint method.

In this paper, a geometrically nonlinear structural model is connected to a Quasi-three-Dimensional (Q3D) NLF aerodynamic solver for SBW aircraft's wing aerostructural analysis and optimization. This tool is capable of accurately, and at the same time computationally efficiently, analyzing and optimizing ultra-high aspect ratio wings with natural laminar flow in the conceptual and preliminary design phase. The coupled tool is integrated into an SBW aircraft conceptual design and optimization framework. In

the case study, an SBW aircraft is initially designed and optimized in the conceptual design stage. Coupled adjoint aerostructural optimization is then performed for the wing of the initially optimized SBW aircraft with the objective function of mission fuel mass.

The rest of this paper is organized as follows: Sec. II presents the methodology for the conceptual design, conceptual optimization, and coupled adjoint aerostructural optimization framework and the verification. An SBW aircraft design case is analyzed and optimized by using the proposed methodology in Sec. IV. Finally, Sec. IV provides a comprehensive conclusion.

II. Methodology

The research on the methodology presented in this section is divided into two aspects: Conceptual Design and Optimization and Coupled Adjoint Aerostructural Optimization. The conceptual design and optimization are performed by using the in-house tool PyInit [41] and the open-source tool SUAVE [42], modified for the purpose of this research, and the aerostructural optimization is performed by using the modified FEMWET code [43]. The design and optimization procedure developed in this work is shown in Fig. 2. Each module and step shown in the figure is explained in detail in the following subsections.

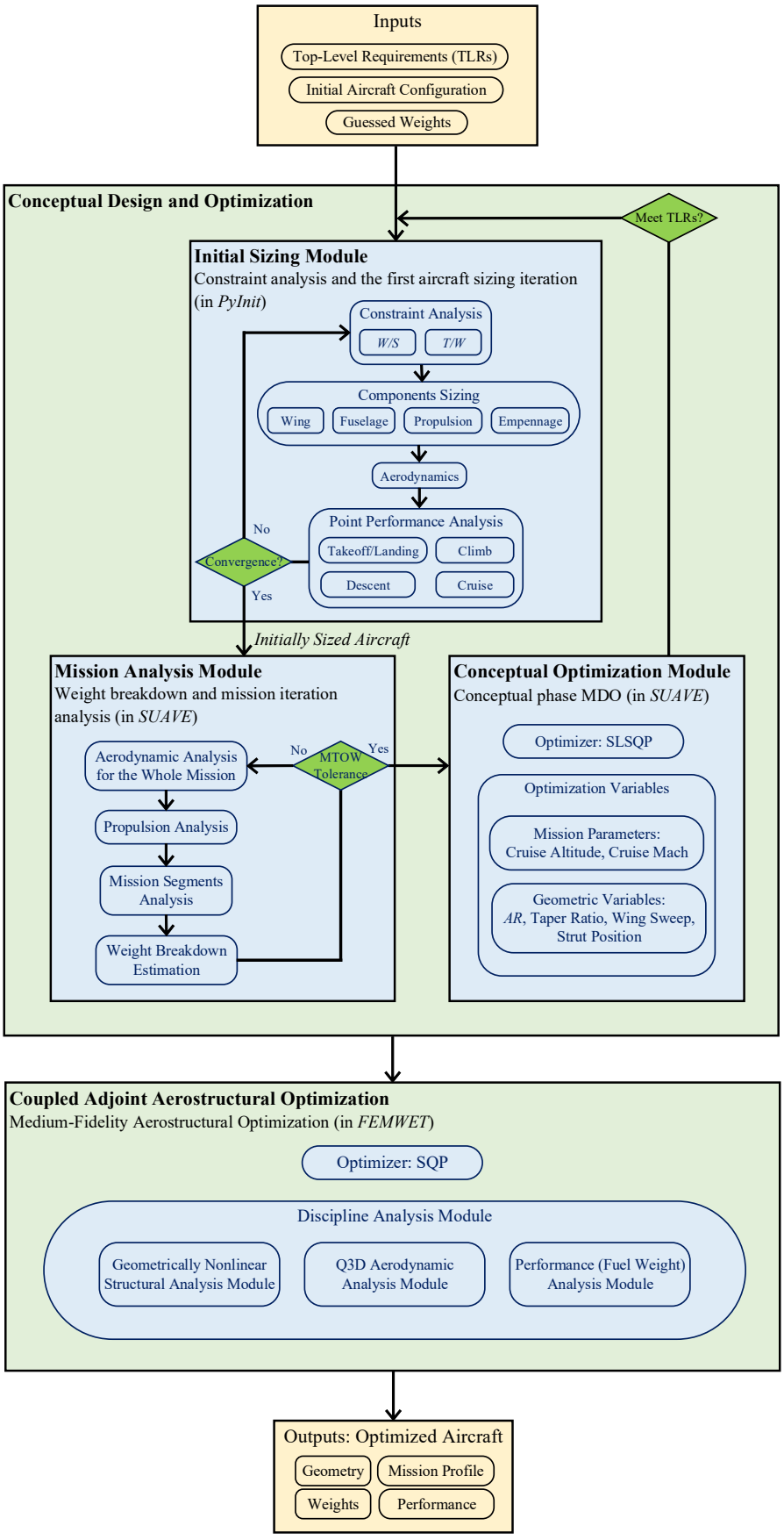

Fig. 2 Design and optimization procedure.

A. Conceptual Design and Optimization Methodology

The aircraft conceptual design and analysis framework consisting of PyInit and modified SUAVE, developed by the authors [41], is employed in this paper. This framework includes the design and analysis modules for SBW aircraft. As illustrated in Fig. 2, the aircraft initial sizing is performed by using the aircraft initial sizing tool PyInit to determine the constraint diagrams and size the components, including wing, strut, fuselage, and tailplanes. Next, the initially sized aircraft is imported into the modified SUAVE (modified for the SBW configuration) for the analysis of mission segments, weight breakdown, aerodynamics, and flight performance through convergent iterations. The target range and mission profile are the inputs to the SUAVE analysis. SUAVE estimates the aircraft fuel consumption in terms of the given aircraft configuration and the required mission profile.

The conceptual design optimization is conducted by using SUAVE optimization infrastructure [44]. The Sequential Least-Squares Programming (SLSQP) algorithm of the SciPy optimization toolbox [45] is used as the optimizer. SUAVE's discipline analysis models are utilized as optimization discipline analysis modules, including mission analysis, aerodynamics, weight estimation, etc. The design variables of the optimization are divided into two categories: mission variables and geometric variables. Mission variables include cruise altitude, cruise Mach number, etc. Geometric variables contain aircraft geometry-related parameters, such as wing *AR*, taper ratio, wing sweep, and wing spanwise strut attachment position.

B. Validation of the Conceptual Design Module

A well-studied SBW aircraft with a high aspect ratio wing, SUGAR [12], was selected for the SBW aircraft analysis module validation. The SUGAR aircraft was designed for the mid-range mission with 154 passengers and a range of 3500 nm, which has been researched in detail by high-fidelity aerodynamic and structural analysis and wind tunnel experiments [46]. The data required for the analysis were

extracted from Ref. [12]. The performance analysis for the SUGAR aircraft was conducted iteratively until the weight and mission segments (including the 3500 nm main flight segment and the required reserve segment) converged. The comparison of the resulted aircraft and SUGAR aircraft at the midpoint of the cruise (i.e., 50% remaining fuel) is listed in Table 1, which shows that the presented conceptual design and analysis method has good accuracy for the weight estimation with relative errors blow 2%. The relatively high error in the aerodynamic data is mainly due to the difference in the drag bookkeeping methods and the supercritical airfoils employed in the SUGAR project and this framework, as described in Ref. [41]. Therefore, a relative difference of around 8% in some aerodynamic data is considered acceptable at the conceptual design stage.

Table 1 Validation of the SBW aircraft performance analysis method

Group	Estimated results	SUGAR [12]	Relative error, %
MTOM, kg	66998	68039	-1.53
Fuel mass, kg	15599	15365	1.52
Empty mass, kg	36799	36328	1.30
C_L	0.685	0.750	-8.67
C_D	0.0290	0.0298	-2.58
L/D	23.5882	25.1590	-6.24

C. Coupled Adjoint Aerostructural Optimization Methodology

The aerostructural optimization of composite, NLF SBW aircraft is performed by using the coupled adjoint aerostructural optimization tool FEMWET [43]. FEWMET is composed of a Q3D aerodynamic solver and a finite beam element structural solver, and the coupled system is solved using the Newton method. A geometrically nonlinear structural model has been developed and integrated into FEMWET in previous work [47]. In this study, FEMWET is modified and applied to the aerostructural optimization study of SBW aircraft.

1. Geometrically Nonlinear Structural Analysis

The structural model is based on composite thin-walled beams with assumptions specific to UHARW, as follows:

- In-plane warping is neglected, i.e., the cross-section may not deform in its plane. For aircraft wings, due to the presence of stiffening members like ribs and stringers, the cross-sectional deformation remains negligible.
- Free warping is assumed for the UHARW. This means that the change of the twist angle with respect to the axial direction of the beam is constant: $\frac{d\varphi}{dz} = \text{Constant}$.
- Small to moderate twist angles are considered in the calculation of the structural response for the SBW as long as the twist angles are small for the aerodynamic performance of the wing. However, the formulation can extend the finite element code to take into account arbitrarily large twist angles.
- Flexural displacements, *u* and *v*, are assumed to be small but finite. Nonlinear terms in the transverse shear strains are omitted, i.e., Von-Karman type strains are considered. The formulation is made based on this assumption for analysis of the aircraft wings under bending loads. However, if other loading types of buckling and post-buckling are going to be investigated, corresponding nonlinear strains can be readily added to the current formulation. In the latter case, the derivative of the lateral wing deflection with respect to the beam axis coordinate (*dw/dz*) will not be small. Therefore, the corresponding higher-order terms are not negligible.
- The transverse shear deformation is considered and added to the in-plane deformation. It is expected that in highly flexible composite UHARW, transverse shear strains are not negligible anymore as assumed in many traditional thin-walled composite beam models in the literature

(Refs. [48, 49]).

The method is briefly explained here and the detailed formulation is presented in Refs. [47, 50].

The kinematic, strain-displacement equations, for the geometrically nonlinear bending of the beam, can be written as:

$$\varepsilon_{zz} = \frac{dw}{dz} + \frac{1}{2}\left[\left(\frac{du}{dz}\right)^2 + \left(\frac{dv}{dz}\right)^2\right]$$
$$\gamma_{sz} = \frac{dw}{ds} + \frac{dv}{dz} \tag{1}$$
$$\gamma_{nz} = \frac{dw}{dn} + \frac{du}{dz}$$

In this formulation, u, v, w are along the x, y, z directions, respectively. The plane x-y resides on the beam cross-section and the axis z is orthogonal to the plane [50]. As it can be seen from the plot in Fig. 3, n and s are normal and tangential coordinates on the contour of the beam. In the same figure, the translational and rotational degrees of freedom are illustrated.

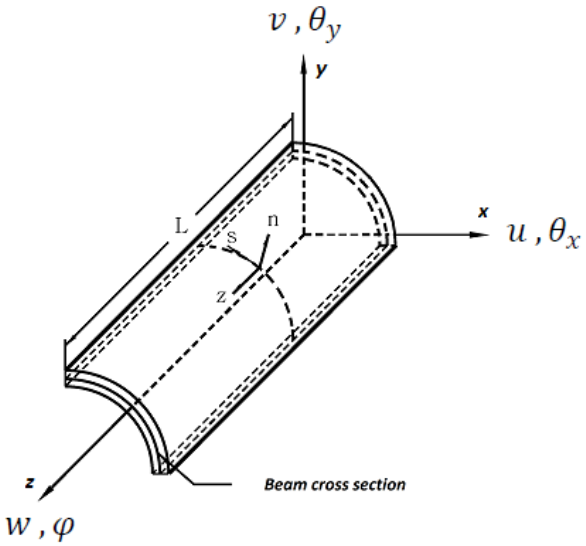

Fig. 3 Cross-sectional coordinates used in the formulation of thin-walled composite wing

As can be seen from Eq. (1), the transverse shear strains are considered in this formulation.

Accordingly, the stress components are formulated as:

$$\begin{Bmatrix}\sigma_{zz}\\ \tau_{sz}\end{Bmatrix}=\begin{bmatrix}Q_{11} & Q_{16}\\ Q_{61} & Q_{66}\end{bmatrix}\begin{Bmatrix}\varepsilon_{zz}\\ \gamma_{sz}\end{Bmatrix};\ \tau_{nz}=Q_{55}\gamma_{nz} \tag{2}$$

Eq.(3) relates the beam force and moment resultants to the generalized beam strains, as

$$\begin{Bmatrix}N_z\\ M_y\\ M_x\\ V_x\\ V_y\\ M_s\\ \Gamma_t\end{Bmatrix}=\begin{bmatrix}E_{11} & E_{12} & E_{13} & E_{14} & E_{15} & E_{16} & E_{17}\\ E_{21} & E_{22} & E_{23} & E_{24} & E_{25} & E_{26} & E_{27}\\ E_{31} & E_{32} & E_{33} & E_{34} & E_{35} & E_{36} & E_{37}\\ E_{41} & E_{42} & E_{43} & E_{44} & E_{45} & E_{46} & E_{47}\\ E_{51} & E_{52} & E_{53} & E_{54} & E_{55} & E_{56} & E_{57}\\ E_{61} & E_{62} & E_{63} & E_{64} & E_{65} & E_{66} & E_{67}\\ E_{71} & E_{72} & E_{73} & E_{74} & E_{75} & E_{76} & E_{77}\end{bmatrix}\begin{Bmatrix}\varepsilon_z^0\\ \kappa_y\\ \kappa_x\\ \gamma_{xz}^0\\ \gamma_{yz}^0\\ \kappa_{sz}\\ \chi_z\end{Bmatrix} \tag{3}$$

The matrix components E_{ij} contain elastic constants and are constructed based on the material and the beam's cross-sectional geometric properties. ε_z is the extensional strain; κ_y and κ_x are the biaxial curvatures in the x and y directions, respectively. χ_z is the higher-order nonlinear (higher-order) curvature, κ_{sz} is the twisting curvature, and Γ_t is the higher-order stress couple due to the twist. Eventually, γ_{xz}^0 and γ_{yz}^0 are the extensional transverse shear strains, respectively.

The generalized strains of the formulated beam, in the reference frame, are defined as:

$$\begin{aligned}\varepsilon_z^0 &= w_{,z}+\frac{1}{2}\left(u_{,z}^2+v_{,z}^2\right)\\ \kappa_y &= \theta_{y,z}+v_{,z}\varphi_{,z}\\ \kappa_x &= \theta_{x,z}+u_{,z}\varphi_{,z}\\ \gamma_{xz}^0 &= u_{,z}+\theta_y\\ \gamma_{yz}^0 &= v_{,z}+\theta_x\\ \kappa_{sz} &= 2\varphi_{,z}\\ \chi_z &= \frac{1}{2}\varphi_{,z}^2\end{aligned} \tag{4}$$

where the symbol (,) in the subscripts means differentiation: $u_{,z}$ means the derivative of u with respect to z, e.g. $u_{,z}=\left(\frac{du}{dz}\right)$.

Subsequently, the finite element equations are obtained for the large displacement analysis of composite thin-walled beams

The proposed method is validated through comparisons to numerical and experimental results available in the literature (see Fig. 4 and Fig. 5). Specifically, for geometrically nonlinear capability verification, the experimental results presented in Refs. [51, 52] are used. The laminate strip is 560 mm long and 30 mm wide and is loaded at 550 mm from the root. Due to the large deflection of the beam, the comparison enables the accuracy of the model for composite beams to be evaluated.

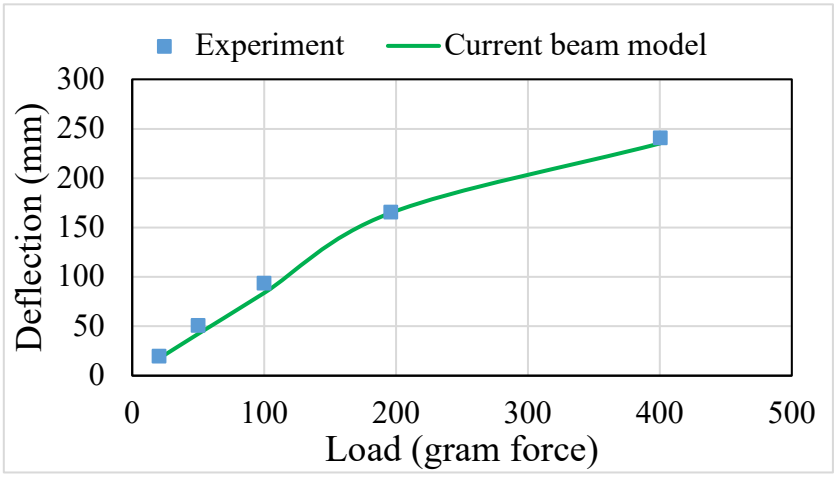

Fig. 4 Deflection of the $[0/90]_{2s}$ composite beam under tip load.

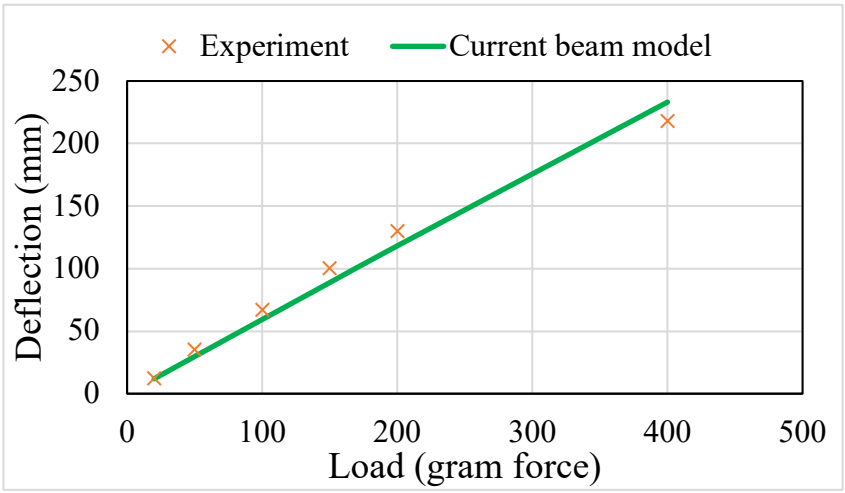

Fig. 5 Deflection of the $[45/0]_{2s}$ composite beam under tip load.

2. Q3D Aerodynamic Analysis for Natural-Laminar-Flow Wings

The Q3D method developed by the authors [53], combining a Vortex Lattice Method (VLM) code and the Two-Dimensional (2D), compressible airfoil analysis tool MSES [54], is utilized for aerodynamic analysis. The VLM code is used to compute the lift coefficient, induced drag, and lift distribution of the wing. The VLM calculations are corrected for the compressibility effect at a high Mach number using Prandtl-Glauert compressibility correction. According to the wing geometry and the angle of attack, the *AIC* matrix and *RHS* vector are calculated and the VLM code is governed by the equation:

$$AIC\ \Gamma = RHS \tag{5}$$

Next, the wing is divided into several sections for 2D aerodynamic analysis. The lift coefficient obtained by using VLM is interpolated to find C_l at each given spanwise section. Sweep theory is employed to calculate C_l, velocity, and Mach number perpendicular to the wing sweep line. Then, MSES is utilized to compute the 2D sectional aerodynamic coefficients. MSES employs the viscous-inviscid-interactive approach. In this method, the Euler inviscid solution is coupled with the integral boundary layer equation and the boundary layer equations are directly solved, as described in Ref. [54]. As illustrated in Fig. 6, the downwash angle (α_i) caused by the wing tip vortex is taken into account in the 2D airfoil analysis to consider the 3D characteristics of the wing in the Q3D method, which is the difference between the free stream and effective velocities. The downwash angle is adjusted during analysis to match the lift coefficient calculated using MSES against that obtained using VLM, and then the viscous, pressure, and wave drag of each section are obtained. Finally, the wing total profile drag is obtained by integrating the 2D sectional drag coefficients along the wingspan. In particular, MSES can calculate the sensitivity of the wing lift and drag with respect to the wing geometry and angle of attack.

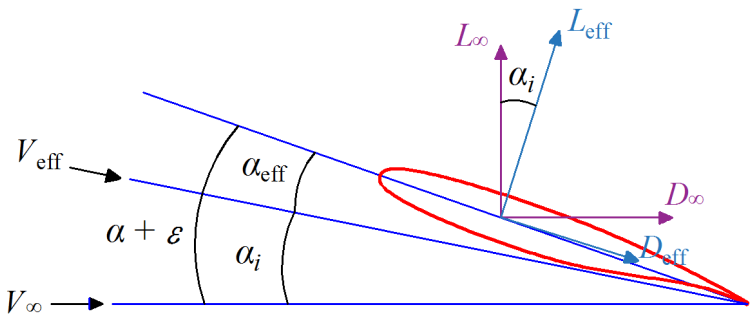

Fig. 6 Angles and aerodynamic forces of a typical 2D wing section

MSES is a medium-fidelity tool that provides a 2D aerodynamic analysis and optimization framework for airfoils [55]. MSES solves the steady Euler equations based on an intrinsic finite-volume grid. The inviscid flow results are coupled with compressible, integral boundary layer formulations featuring envelop e^N boundary layer transition prediction criterion through the displacement thickness and edge velocity. Newton method is utilized to solve the system of equations. This linear stability theory e^N method determines the amplitude of the highest Tollmien-Schlichting wave frequency at each point. Once the growth rate is obtained, the e^N criterion is employed to determine transition points. Based on this method, MSES can predict the laminar-to-turbulent transition points of airfoils and thus calculate the airfoil lift and drag coefficients, i.e., free-transition mode. In this research, FEMWET utilizes the free-transition mode of MSES to perform the aerostructural optimization for NLF wings.

3. Aerostructural Coupling

The proposed geometrically nonlinear structure and Q3D aerodynamic modules are integrated to solve the coupled physics problem of flexible high aspect ratio wings by using the Newton method, as shown in Eq. (6). The coupled aerostructural system, i.e., aerodynamic loads and structural deformation, is characterized by the following system of governing equations:

$$\begin{bmatrix} A(X,\ \Gamma,\ U,\ \alpha) \\ S(X,\ \Gamma,\ U) \\ W(X,\ \Gamma) \\ C(X,\ \Gamma,\ U,\ \alpha,\ \alpha_i) \end{bmatrix} = 0 \tag{6}$$

The first two equations in Eq.(6) are the governing equations of the VLM and FEM, respectively. The third equation represents that the lift should be equal to the design load factor multiplied by the design weight, which determines the angle of attack of the wing. The last equation indicates that the 2D sectional lift computed by MSES should be equal to the lift calculated using the VLM (corrected for the wing sweep). The Newton method is used to solve Eq. (6). The state variables [Γ, U, α, α_i] are updated iteratively as follows until Eq. (6) is satisfied (with a defined tolerance)

$$\Delta \begin{bmatrix} \Gamma \\ U \\ \alpha \\ \alpha_i \end{bmatrix} = - \begin{bmatrix} \frac{\partial A}{\partial \Gamma} & \frac{\partial A}{\partial U} & \frac{\partial A}{\partial \alpha} & \frac{\partial A}{\partial \alpha_i} \\ \frac{\partial S}{\partial \Gamma} & \frac{\partial S}{\partial U} & \frac{\partial S}{\partial \alpha} & \frac{\partial S}{\partial \alpha_i} \\ \frac{\partial W}{\partial \Gamma} & \frac{\partial W}{\partial U} & \frac{\partial W}{\partial \alpha} & \frac{\partial W}{\partial \alpha_i} \\ \frac{\partial C}{\partial \Gamma} & \frac{\partial C}{\partial U} & \frac{\partial C}{\partial \alpha} & \frac{\partial C}{\partial \alpha_i} \end{bmatrix} \begin{bmatrix} A \\ S \\ W \\ C \end{bmatrix} \tag{7}$$

It should be noted that the loads are computed and transformed on the deformed geometry at each Newton iteration.

The aileron effectiveness is an important constraint in aerostructural optimization, especially for the high aspect ratio wing configuration because the optimization results may have problems such as aileron reversal if this constraint was not taken into account [56]. It is defined as the ratio of elastic to rigid roll moment of the wing due to aileron deflections, which can be expressed as

$$\eta_\alpha = \frac{L_{\delta_{\text{elastic}}}}{L_{\delta_{\text{rigid}}}} \tag{8}$$

The aileron deflection is simulated in the VLM code.

4. Sensitivity Analysis

The aerostructural optimization is conducted using a gradient-based optimization algorithm. The coupled adjoint derivative calculation method is used to compute the total sensitivity of any function, for example, structural failure criteria with respect to the design variables like the thickness of the wing box equivalent panels. The total sensitivity of a function I with respect to a design variable X is calculated as

$$\frac{\mathrm{d}I}{\mathrm{d}X}=\frac{\partial I}{\partial X}+\frac{\partial I}{\partial Y}\frac{\mathrm{d}Y}{\mathrm{d}X} \tag{9}$$

For the coupled system of the aerostructural optimization problem studied in this work, as shown in Eq.(6), Eq.(9) can be expressed as

$$\frac{\mathrm{d}I}{\mathrm{d}X}=\frac{\partial I}{\partial X}-\varphi_1^T\left(\frac{\partial A}{\partial X}\right)-\varphi_2^T\left(\frac{\partial S}{\partial X}\right)-\varphi_3^T\left(\frac{\partial W}{\partial X}\right)-\varphi_4^T\left(\frac{\partial C}{\partial X}\right) \tag{10}$$

where $\varphi=\left[\varphi_1\ \varphi_2\ \varphi_3\ \varphi_4\right]^T$ is the adjoint vector which is calculated using the following equation:

$$\begin{bmatrix} \frac{\partial A}{\partial \Gamma} & \frac{\partial A}{\partial U} & \frac{\partial A}{\partial \alpha} & \frac{\partial A}{\partial \alpha_i} \\ \frac{\partial S}{\partial \Gamma} & \frac{\partial S}{\partial U} & \frac{\partial S}{\partial \alpha} & \frac{\partial S}{\partial \alpha_i} \\ \frac{\partial W}{\partial \Gamma} & \frac{\partial W}{\partial U} & \frac{\partial W}{\partial \alpha} & \frac{\partial W}{\partial \alpha_i} \\ \frac{\partial C}{\partial \Gamma} & \frac{\partial C}{\partial U} & \frac{\partial C}{\partial \alpha} & \frac{\partial C}{\partial \alpha_i} \end{bmatrix}^T \begin{bmatrix} \varphi_1 \\ \varphi_2 \\ \varphi_3 \\ \varphi_4 \end{bmatrix} = \begin{bmatrix} \frac{\partial I}{\partial \Gamma} \\ \frac{\partial I}{\partial u} \\ \frac{\partial I}{\partial \alpha} \\ \frac{\partial I}{\partial \alpha_i} \end{bmatrix} \tag{11}$$

The partial derivatives of the governing equations with respect to the state variables in Eq.(11) have been computed in the Newton iteration. All the partial derivatives are calculated by a combination of analytical methods and automatic differentiation. The automatic differentiation is conducted using the Matlab toolbox Intlab [57]. Besides, the derivatives of the 2D aerodynamic coefficients are provided by MSES.

5. Performance Analysis

The fuel mass is estimated using the semi-empirical method presented by Roskam [58]. In this method, the cruise-required fuel mass is calculated using the Breguet range equation and statistical factors are employed to estimate the fuel mass for the other flight segments. The fuel mass is calculated by

$$m_F = k_R \left(1 - M_{ff}\right) MTOW \tag{12}$$

The aircraft lift-to-drag ratio is required for the calculation of M_{ff}. To compute the lift-to-drag ratio, the aircraft's total drag is assumed to be the sum of the wing drag and the drag of the rest of the aircraft. The wing drag is calculated according to the design variables, while the remaining drag (at the cruising angle of attack) is kept constant during the optimization, which comes from the above-introduced conceptual design optimization results.

6. Validation

FEMWET has been validated in terms of different aspects in previous studies. The accuracy of the Q3D aerodynamic solver has been verified with MATRICS-V code, a CFD tool with higher fidelity, as presented in Ref. [53]. The wing twist of the A320-200 aircraft under +1g load was utilized to validate the accuracy of FEMWET for calculating the wing stiffness and deformation, and FEMWET presented an error of -0.12% in the wing weight estimation through performing an aeroelastic optimization [43].

According to the above-mentioned validations, the accuracy and efficiency of FEMWET can be validated. However, the FEMWET is modified to perform aerostructural optimization of the SBW configuration in this paper, therefore, additional validations for the modified FEMWET are necessary. The wing of the A320 aircraft was employed to verify the correct implementation of the composite version of FEMWET. A Quasi-Isotropic (QI) layup was adopted for the wing box equivalent panels. The rest of the wing was kept the same as the original aircraft. The QI layups utilized for the wing box are $[0 / 45 / -45 / 90]_s$ and the material properties used are given in Table 2, which refers to Ref. [59]. An aeroelastic optimization is performed to size the thickness of the equivalent panels according to five different load cases (see Table 3). The optimization results of the A320 wing with QI layup are shown in Table 4. It should be mentioned that the optimized QI composite wing is 2.02% heavier than the actual

A320 aluminum (Al) wing, which is consistent with the findings in the literature that the QI layups generally result in the same or slightly heavier wing as the Al material [20, 60].

Table 2 Material properties for the composite layers

E_1, GPa	E_2=E_3, GPa	G_{12}=G_{13}, GPa	G_{23}, GPa	ν_{12}=ν_{13}
146.78	10.3	6.2	4.8	0.28

Table 3 Load cases of A320 wing aeroelastic optimization

Load case	Type	H, m	Mach	n, g
1	Pull up	7500	0.89	+2.5
2	Pull up	0	0.58	+2.5
3	Push down	7500	0.89	-1.0
4	Roll motion	4000	0.83	+1.0
5	Cruise	11000	0.82	+1.0

Table 4 A320 wing mass estimation

Category	Optimized for QI	Optimized for Al [43]	Actual A320 wing	Relative error		
				QI w.r.t. A320	Al w.r.t. A320	QI w.r.t. Al
Wing mass	8968.3 kg	8790.8 kg	8801 kg	+1.9 %	-0.1 %	+2.02 %

III. Case Study

In this section, a medium-range SBW aircraft with a similar mission to the A320 is initially designed and optimized. Then, aerostructural optimization is performed for the wing of the initially optimized aircraft by using the presented FEMWET tool.

A. SBW Aircraft Conceptual Design and Optimization

An MR-SBW aircraft with a similar mission to the A320 was initially designed by the authors, as presented in Ref. [41]. This MR-SBW aircraft was designed to operate at Mach 0.78 with 150 passengers

(2 class). Uncertainty analysis and constrained optimization were conducted for this aircraft with the objective function of the mission fuel mass [61]. The uncertainty analysis results showed that the MR-SBW aircraft has the highest fuel efficiency operating at a cruise Mach number of 0.735 (uncertainty bounds are Ma=0.71 to Ma=0.78). Furthermore, this relatively low Mach number facilitates the NLF realization over the wing, thus further improving the aircraft's fuel efficiency. Therefore, an MR-SBW aircraft similar to the one designed in Ref. [41] but operating at Mach 0.735 is designed in this paper (i.e., Baseline Configuration in Fig. 7) before performing conceptual optimization (i.e., Reference Configuration in Fig. 7) and aerostructural optimization (i.e., Configurations A and B in Fig. 7). It should be mentioned that the MR-SBW aircraft is designed with NLF assumptions at the conceptual design stage (i.e., Baseline Configuration and Reference Configuration). The conceptually optimized configuration (Reference Configuration) is then reanalyzed in SUAVE by excluding NLF assumptions for the subsequently triggered transition mode aerostructural optimization, which is named Reference B, and its data are given in Table 13.

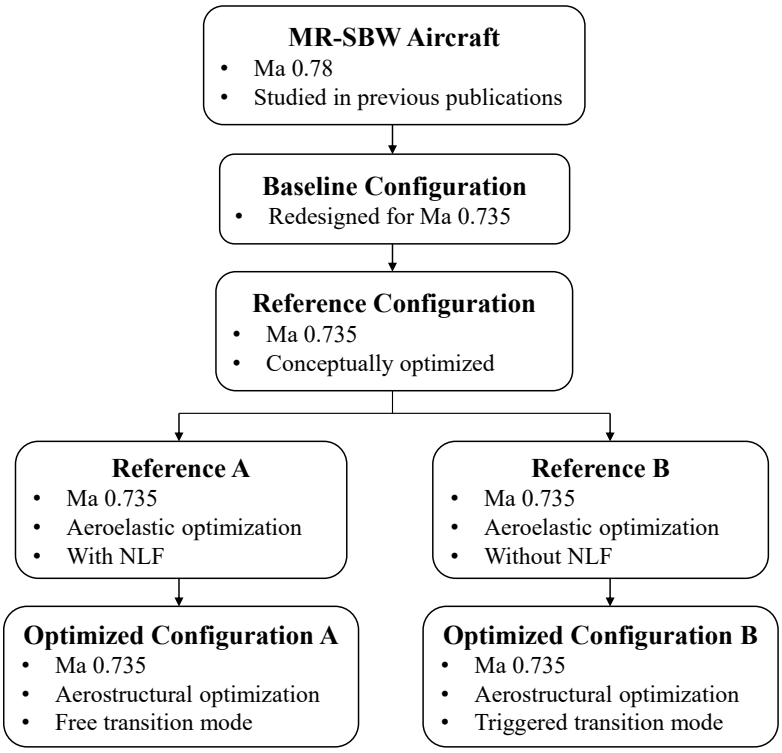

Fig. 7 Illustration of the configurations studied in this work

The top-level aircraft requirements for the baseline configuration are given in Table 5. It should be mentioned that since the MR-SBW aircraft is designed to operate in the entry-into-service year of 2040, it is assumed that the maximum load factor requirement can be released to +1.5g to -0.5g due to the application of advanced load alleviation technologies [41, 62]. The conceptual design module shown in Fig. 2, composed of PyInit and SUAVE, was utilized for the initial sizing and performance analysis of the MR-SBW aircraft. Tthe semi-empirical wing weight estimation method for SBW aircraft developed by Chiozzotto [63] was used during the conceptual design stage. The wing mass penalty of the wing folding mechanism was estimated using the method presented in Ref. [64]. The initially sized MR-SBW aircraft is visualized using OpenVSP, as shown in Fig. 8. The wing geometry parameters and mass breakdown of the sized aircraft are listed in Table 6 and Table 7, respectively.

Table 5 Top-level aircraft requirement

Parameter		Unit	Value
Cruise Mach		--	0.735
Max. Mach		--	0.78
Passengers (2-class)		--	150
Range		nm	3400
Reserves	Contingency fuel	--	3%
	Divert segment	nm	200
	Hold (at 1500 ft)	min	10
Cruise altitude		ft	33000
Service ceiling		ft	38500
Takeoff field length		ft	<6400
Landing distance		ft	<4500
Wingspan		ft	<118

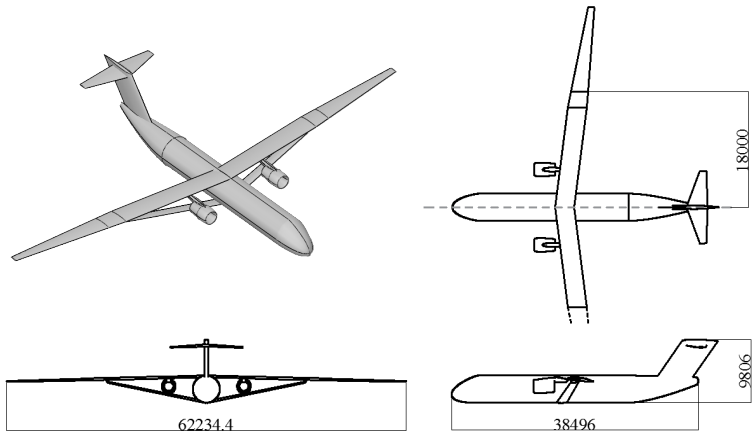

Fig. 8 MR-SBW aircraft

Table 6 Wing geometry parameters of the MR-SBW aircraft

Parameter	Value
Aspect ratio	25
Quarter-chord sweep, deg	7.5
Span, m	62.2344
Taper ratio	0.35
Folding position, m	18
Dihedral, deg	-1.5
Strut span, m	31.1201

Table 7 Mass breakdown of the MR-SBW aircraft

Parameter	MR-SBW	A320neo
MTOM, kg	67623	79000
Fuel mass, kg	16644	20980
OEM, kg	36759	44300
Empty mass breakdown		
SBW, kg	8818	
Fuselage, kg	7066	
Propulsion, kg	4783	
Landing gear, kg	2282	
Horizontal tail, kg	479	
Vertical tail, kg	896	
Paint, kg	449	
System, kg	11986	

As shown in Table 7, although the initially designed MR-SBW aircraft shows significant benefits compared to the reference A320neo aircraft, conceptual optimization study was performed to further improve its fuel efficiency. As illustrated in Fig. 2, the SUAVE optimization infrastructure was used for the conceptual optimization of the MR-SBW aircraft. The goal of the optimization is to minimize the mission fuel mass with respect to the wing and strut design variables. Wing aspect ratio, taper ratio, quarter-chord sweep angle, and strut attachment position were selected as design variables. The optimization constraints include the design variables' bounds and the top-level aircraft requirements. The optimization problem is defined as:

$$
\begin{aligned}
&\text{minimize} && W_F(X) \\
&\text{w.r.t.} && X=\left[AR,\ \lambda,\ \Lambda,\ \eta_{st}\right] \\
&\text{subject to} && 20 \le \mathrm{AR} \le 30 \\
& && 0.30 \le \lambda \le 0.65 \\
& && 5 \le \Lambda \le 15 \\
& && 0.40 \le \eta_{st} \le 0.60 \\
& && h_i(X) = 0 \qquad i = 1..n \\
& && g_j(X) = 0 \qquad j = 1..m
\end{aligned}
\tag{13}
$$

where h and g are equality and inequality constraints determined by the top-level aircraft requirements

listed in Table 5, including cruise Mach, maximum Mach, flight mission profile, range, etc.

The conceptual optimization results of the MR-SBW aircraft are shown in Table 8 and Fig. 9. The SLSQP algorithm of the SciPy optimization toolbox was employed as the optimizer. The MR-SBW aircraft was optimized for fuel mass throughout the mission profile, including takeoff, climb, cruise, descent, and reverse segments. After optimization, the fuel mass was reduced by 3.17%. The wing sweep angle was increased from 7.50 deg to 10.54 deg because wave drag still existed on the wing when the Mach number was reduced to 0.735. It is noteworthy that the compressibility drag is computed by calculating the crest critical and divergence Mach numbers in SUAVE using the semi-empirical method presented in Ref. [65]. The initially optimized MR-SBW aircraft will be utilized as the reference configuration for aerostructural optimization in FEMWET.

Table 8 Conceptual optimization results for the MR-SBW aircraft

Parameter	Baseline	Optimization result (Reference Configuration)	Difference, %
AR	25.00	25.81	3.24
λ	0.35	0.43	22.86
Λ, deg	7.50	10.54	40.53
η_{st}	0.5000	0.4865	-2.70
m_F, kg	16644	16117	-3.17
MTOM, kg	67623	67262	-0.53
OEM, kg	36759	36925	0.45

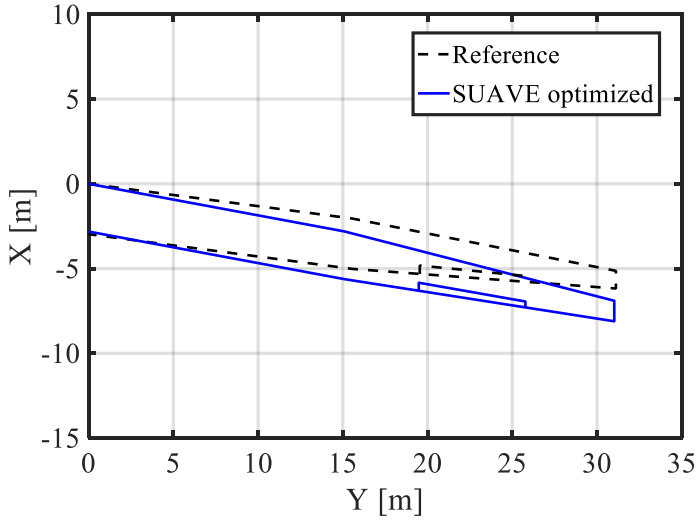

Fig. 9 Wing planform comparison of SUAVE optimization

B. Coupled Adjoint Aerostructural Optimization

In this section, the FEMWET is used to perform aerostructural optimization for the wing and strut of the initially optimized MR-SBW aircraft. The SBW configuration implementation in FEMWET, the optimization problem definition, and aerostructural optimization results are presented in the following subsections.

1. SBW configuration implementation in FEMWET

The FEWMET tool was originally developed for conventional cantilever wing aircraft [43]. Therefore, the FEMWET needs to be modified to take into account the additional strut component and the combination between the wing and the strut.

The strut could be designed as a lifting surface to carry part of the wing's load, but this would need to be investigated at the aircraft level to determine whether the load-carrying strut design would benefit the aircraft. NASA funded research on the load-carrying strut design of SBW aircraft and concluded that the strut is better served as a purely structural component with trimming to limit its drag contribution

[66], while strut loading design may be beneficial for higher Mach number (e.g., Mach=0.80) SBW aircraft by reducing the likelihood of shocks forming on the wing [46]. Therefore, the strut of the MR-SBW aircraft is designed as a purely structural member, without contributing to the wing lift.

In FEMWET, finite beam elements are utilized to model the structure of the wing and strut. The wing and strut are replaced by a beam placed at the wing box elastic axis, respectively. The strut beam is connected to the corresponding wing beam node at the strut attachment position. Aerostructural coupling requires the transfer of displacements from the structural solver to the aerodynamic solver and the transfer of aerodynamic loads from the aerodynamic solver to the structural solver. Interpolation techniques are used in FEMWET for this information transformation. Fig. 10 shows an example of the VLM mesh for the wing and the equivalent beam models of the wing and the strut. In this paper, the aerodynamic and structural grids are mapped in the way shown in Fig. 10 to avoid interpolation.

The wing geometry is shown in Fig. 11. The strut attachment position is defined at 48.65% of the wing semi-span according to the conceptual optimization results. Besides, the fuel tank length is limited by the wing folding position to reduce the weight penalty due to wing folding. Therefore, the available fuel volume needs to be a constraint in the aerostructural optimization (assume all the fuel is in the wing fuel tanks).

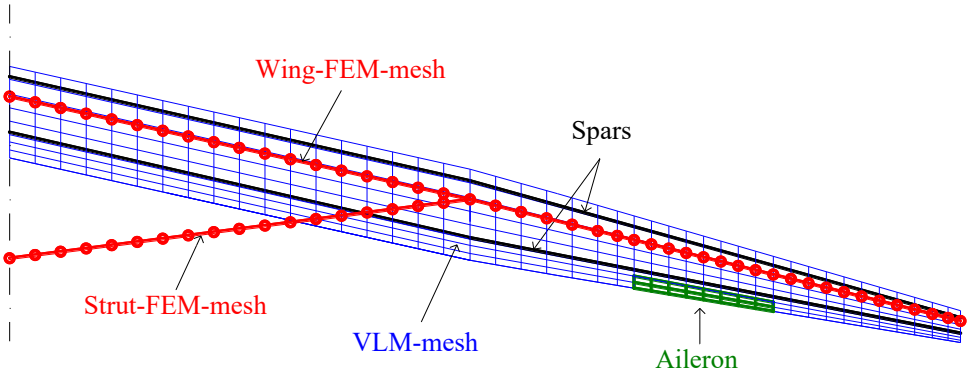

Fig. 10 Example of an aerodynamic and structural mesh

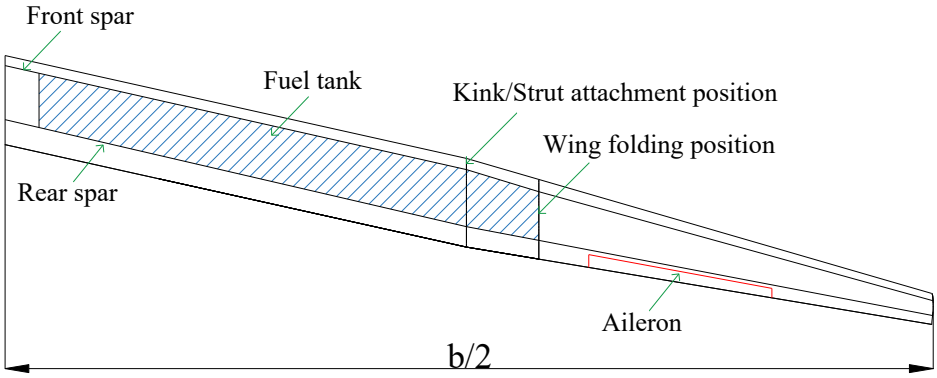

Fig. 11 Schematic of the MR-SBW aircraft wing

The load cases employed in the aerostructural optimization are given in Table 9, which are determined to correspond to the flight envelope and load diagram studied in the conceptual design phase. It should be mentioned that only a single point in the cruise segment (midpoint) is considered in this work, as a recent study by Adler and Martins [67] showed that the difference in fuel consumption between single-point and multi-point optimization results was less than 0.05% for a B737-800-like aircraft with mission ranges greater than 2900 nm.

Table 9 Load cases of the MR-SBW aircraft

Load case	Type	Weight	H [m]	Ma	n [g]
1	Pull-up	W_{TO}	7500	0.78	1.5
2	Pull-up	W_{TO}	0	0.58	1.5
3	Push-down	W_{TO}	7500	0.78	-0.5
4	Roll	W_{des}	4000	0.75	1
5	Cruise	W_{des}	10058	0.735	1

*W_{des} is the aircraft design weight, i.e., the mid-cruise weight.

The wing of the MR-SBW aircraft presented above was utilized to verify the sensitivity analysis method of the geometrically nonlinear structural FEMWET. The equivalent beam modeling approach for the wing and strut and the parameterization method for the wing airfoils are introduced in Section II. The finite difference method was used to check the adjoint method adopted in FEMWET. The comparison of the sensitivity of C_D with respect to airfoil shape, parameterized using Chebyshev polynomials, and the sensitivity of wing and strut weight with respect to wing box panels' thicknesses in the adjoint method and finite difference method is shown in Fig. 12. The maximum and minimum of the absolute error and relative error of the sensitivities are calculated and given in Table 10. The absolute error is calculated by $\varepsilon = \left| f'_{\text{adjoint}} - f'_{\text{finite}} \right|$, and the relative error is defined as $\varepsilon_r = \left| f'_{\text{adjoint}} - f'_{\text{finite}} \right| / \left| f'_{\text{finite}} \right|$. Both the relative error and absolute error are less than 10^{-2}, showing the good accuracy of the proposed adjoint sensitivity computation method.

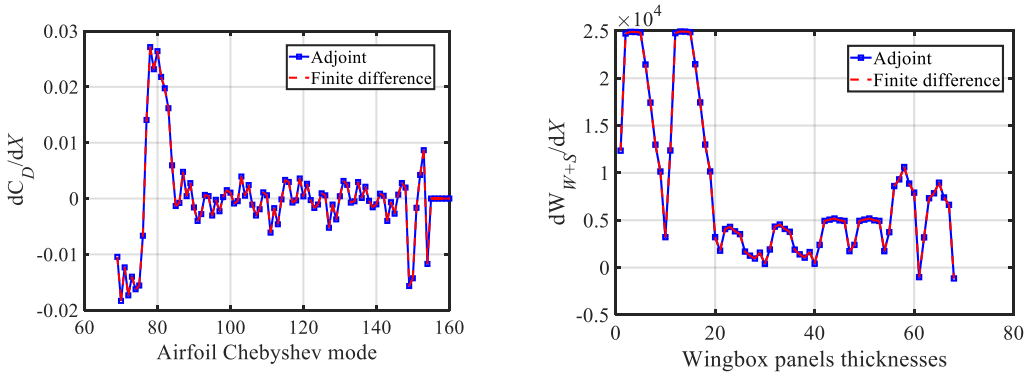

a) **b)**

Fig. 12 Verification of the sensitivity analysis: a) wing drag coefficient w.r.t. Chebyshev modes; b) wing and strut weight w.r.t. wing panels thicknesses

Table 10 Verification of the sensitivity analysis results

Derivative	Absolute error		Relative error	
	Max.	Min.	Max.	Min.
dW_{W+S}/dX	5.0333e-6	8.0487e-8	2.9005e-9	3.8692e-12
dC_D/dX	2.9583e-6	4.0121e-10	0.0011	2.1524e-6

2. Optimization Problem Definition

In order to start the full aerostructural optimization from a feasible starting point (to achieve a better convergence), two optimization problems are solved in this work. First, an aeroelastic optimization is conducted to obtain the initial values of the structural design variables, i.e., the thickness of the wing box panels and spars for the initial wing geometry. The full aerostructural optimization is then carried out from the feasible initial structure.

Aeroelastic Optimization Problem:

The objective of the aeroelastic optimization is to minimize the wing and strut structural mass while ensuring that the structure satisfies the failure constraints under the specified load cases. For the aeroelastic optimization, all aircraft parameters are kept constant except for structural variables. In this work, a quasi-isotropic layup is chosen and the optimization changes the thickness and the corresponding

number of layers but the overall layup (fiber angles) remains constant. The optimization problem is defined as:

$$\begin{aligned} &\text{minimize} && W_{W+S}(X) \\ &\text{w.r.t.} && X=\left[t_{u_i},\ t_{l_i},\ t_{fs_i},\ t_{rs_i}\right] \\ &\text{subject to} && \text{Failure}_k \le 0 \\ & && 1-L_\delta / L_{\delta,\min} \le 0 \\ & && X_{lower} \le X \le X_{upper} \end{aligned} \tag{14}$$

The wing and strut are divided into 15 and 7 trunks along the span with four panels, including the upper, lower, front spar, and rear spar. Therefore, in total 88 design variables are used. Each equivalent panel is divided into four elements for the stress and failure criteria calculation. Each spar panel is divided into two elements for the same reason. The failure criteria include failure under tension, compression, as well as Euler and shear buckling. In total, 3072 constraints on the structural failure (corresponding to the load cases listed in Table 9) and one constraint on the aileron effectiveness are utilized. L_δ and $L_{\delta,\min}$ are respectively the derivative of the roll moment due to aileron deflection for the wing and the minimum required value to satisfy the roll requirements based on the regulations [68]. In this paper, Roskam's semi-empirical method [69] was employed to compute the aircraft's moment of inertia, and Sadraey's method [68] was utilized to calculate the required minimum L_δ.

Aerostructural Optimization Problem:

The objective of aerostructural optimization is to minimize the mission fuel mass according to Eq.(12). The aerostructural optimization problem is defined as:

$$
\begin{aligned}
&\text{minimize} && m_F\left(X\right)\\
&\text{w.r.t.} && X=\left[t_{u_i},\ t_{l_i},\ t_{fs_i},\ t_{rs_i},\ G,\ G_{st},\ P,\ m_{FS},\ MTOW_S\right]\\
&\text{subject to} && \text{Failure}_k \le 0\\
& && 1-L_\delta / L_{\delta,\min} \le 0\\
& && \frac{MTOW / S_w}{MTOW_0 / S_{w0}} - 1 \le 0\\
& && \frac{W_F}{W_{FA}} - 1 \le 0\\
& && \frac{W_F}{W_{FS}} - 1 = 0\\
& && \frac{MTOW}{MOTW_S} - 1 = 0\\
& && X_{lower} \le X \le X_{upper}
\end{aligned}
\tag{15}
$$

The design variables for aerostructural optimization consist of four groups. The design variables of the first group are the thickness of the wing and strut structural panels and spars. The second group of design variables is utilized to define the wing and strut airfoils shape. The airfoil shape at each spanwise position is parameterized by using Chebyshev polynomials. 10 modes are used for each airfoil surface, and therefore 20 modes per airfoil. A total of 100 variables of the G vector is employed to take into account 5 wing sections equidistantly distributed along the wing. As the strut is designed for a non-lift surface and symmetric airfoils are used for the strut, only the thickness-to-chord ratios of the 5 strut airfoils are selected as design variables, i.e., G_{st} vector. The wing planform geometry is parameterized by the third group P through 14 design variables, including root chord, wingspan, taper ratio, leading-edge sweep angle, and 10 twists evenly distributed along the wingspan. In the fourth group, two surrogate values are used for aircraft MTOW and fuel mass, to avoid iterations for convergence on weight. In this way the optimizer is responsible for satisfying the consistency of the design and no iteration at the analysis level is needed for weight. As both MTOW and fuel mass are defined as design variables, their initial values are defined based on the results of the conceptual design (SUAVE) similar to the other design variables. Then the optimizer updates those values in the same way as the other design variables

to satisfy the two consistency constraints, which enforce that the surrogate values for MTOW and fuel mass should be equal to the actual values of MTOW and fuel mass coming from the analysis. In summary, a total of 209 design variables are included in the aerostructural optimization problem, as listed in Table 11.

Table 11 Number of design variables for the aerostructural optimization

Design variable	Number
Thicknesses of the upper panel (wing & strut)	22
Thicknesses of the lower panel (wing & strut)	22
Thicknesses of the front spar (wing & strut)	22
Thicknesses of the rear spar (wing & strut)	22
Wing airfoil Chebyshev polynomials	100
Strut airfoils' thickness-to-chord ratio	5
Wing planform geometry	14
Surrogate variable	2
Total	209

In addition to the 3 groups of constraints in aeroelastic optimization, 4 new constraints are introduced in aerostructural optimization. $\frac{MTOW / S_w}{MTOW_0 / S_{w0}} - 1 \le 0$ represents the wing loading, defined as MTOM divided by the wing reference area, which should not exceed the wing loading of the initial wing, thus keeping the optimized aircraft capable of satisfying the takeoff and landing requirements listed in Table 5. $\frac{m_F}{m_{FA}} - 1 \le 0$ means that the required mission fuel mass should be less than the available fuel mass (related to the fuel tank volume). The two equality constraints state that the calculated values of mission fuel mass and MTOM should be equal to their surrogate values, as explained above. The number of constraints for the aerostructural optimization is given in Table 12.

From Table 11 and Table 12 one can observe that the number of constraints is more than the number of design variables. In such cases, the direct method is more efficient than the adjoint method for

sensitivity analysis. In this project, we initially developed the code based on the constraint aggregation technique and the adjoint method, which is more efficient when the number of design variables is larger than the number of constraints. However, after running the code, we realized that the computational efficiency of the code is very high, so to increase the robustness of the optimization we directly used all the constraints rather than aggregating then, while the cost of the adjoint method was still affordable (in fact the CPU time for solving the 3077 adjoint equations, in this case, was less than 3 seconds).

Table 12 Number of constraints for the aerostructural optimization

Constraint	Number
Tension	768
Compression	768
Buckling	1536
Aileron effectiveness	1
Wing loading	1
Fuel volume	1
Surrogate values	2
Total	3077

3. Aerostructural Optimization

The sequential quadratic optimization algorithm of the Matlab optimization toolbox was utilized as the optimizer. The optimality tolerance, function tolerance, and constraint tolerance are all set to 1e-6 as the termination criteria for optimization. The SUAVE optimization results shown in Table 8 were used as input for FEMWET optimization. Firstly, an aeroelastic optimization was performed for the wing and strut of the SBW aircraft to obtain reasonable thicknesses of structural panels and spars. The aeroelastically optimized SBW mass is given in Table 13, which is notably heavier than the SUAVE (i.e., empirical method) estimated value. This is mainly because the aileron effectiveness constraint is an active

constraint in the aeroelastic optimization of UHARW. As illustrated in Fig. 13, the aeroelastic optimization results without considering the aileron effectiveness constraint are quite close to the semi-empirical method employed in this study, while the wing mass has to be increased significantly to meet the aileron effectiveness constraint.

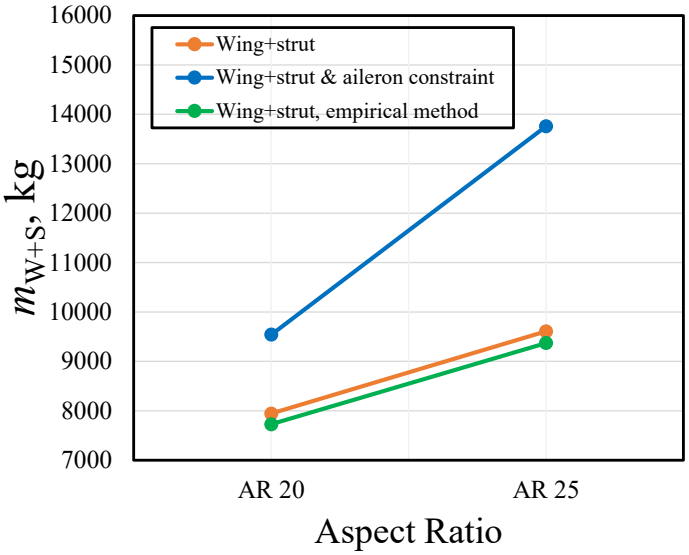

Fig. 13 SBW mass comparison of different methods ("orange" represents the aeroelastic optimization under +1.5 g and -0.5 g, "blue" represents the aeroelastic optimization including the aileron effectiveness constraint, and "green" represents the semi-empirical method estimated results)

The aerostructural optimization was conducted based on the SBW configuration shown in Table 8 and Fig. 11 and the structural inputs obtained from the aeroelastic optimization. It should be mentioned that the aeroelastic optimization resulted in a considerably heavier wing than the conceptual design results (see Fig. 13 for the reason), which was used as the starting point for the aerostructural optimization. The aerostructural optimization was performed in free-transition mode to take into account the flow

transition of the wing starting with the transonic NLF airfoil presented in Ref. [70]. For comparison, another aerostructural optimization was conducted starting with the same airfoils, but with triggered transition mode, i.e., the flow transition is triggered at 2% of the chord from the wing leading edge, to have a full turbulent design.

The optimization histories are shown in Fig. 14 and the optimization results are given in Table 13. In boundary layer free transition mode optimization (Optimized A), the optimized SBW resulted in more than 10% lower fuel mass, more than 8% reduction in aircraft MTOM, and more than 30% reduction in wing and strut structural weight. The optimizer reduced the wing sweep angle (from 10.54 deg to 8.88 deg) by reducing the wave drag through removing/weakening shock waves (see Fig. 15 and Fig. 16). Moreover, as listed in Table 14, the wing friction drag was reduced by more than 56% in free transition mode optimization, because the wing airfoils were optimized to expand the laminar flow boundary layer range. As shown in Fig. 17, the optimized wing's laminar boundary layer range on the wing upper surface was improved by about 10%, while a more significant improvement of the laminar boundary layer range is found on the wing lower surface, which was increased by more than 200% inside the aileron and more than 100% outside the aileron along the wingspan.

In the free transition mode optimization, the NLF is computed in the 2D airfoil analysis tool MSES and it is assumed that the NLF is freely achievable from the wing root to the wing tip. In practice, however, it is difficult to maintain NLF at the wing root and wing tip. If assuming the body boundary conditions were fully turbulent and the free transition model is applied to the flow on the upper and lower surfaces of the wing from 10% span to 90% span, the fuel mass is 14546 kg (0.97% difference from 14406 kg in Table 13).

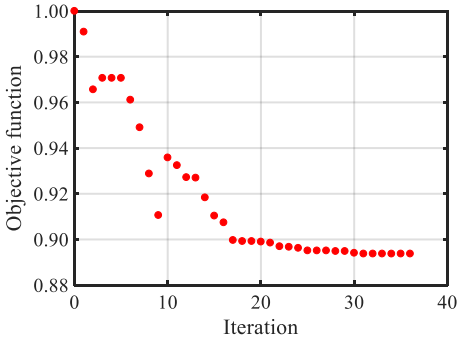

a) Objective function (free transition)

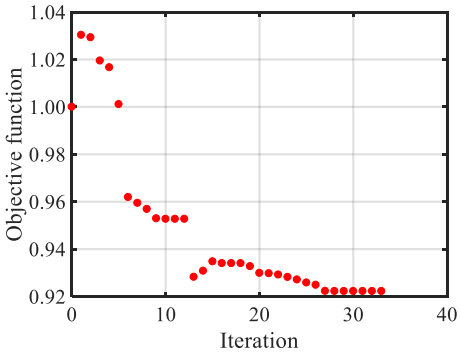

b) Objective function (triggered transition)

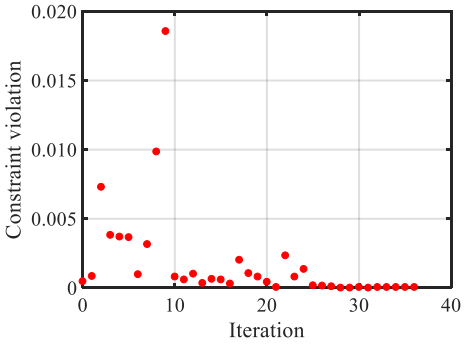

c) Constraint violation (free transition)

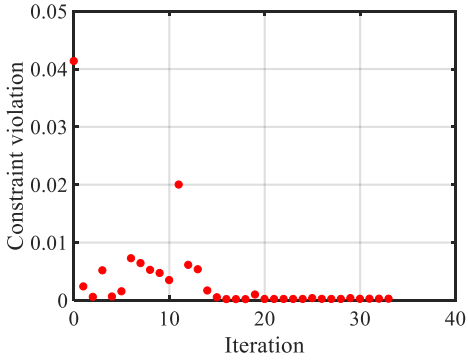

d) Constraint violation (triggered transition)

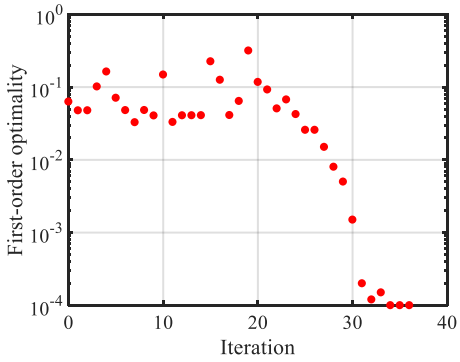

e) Fist order optimality (free transition)

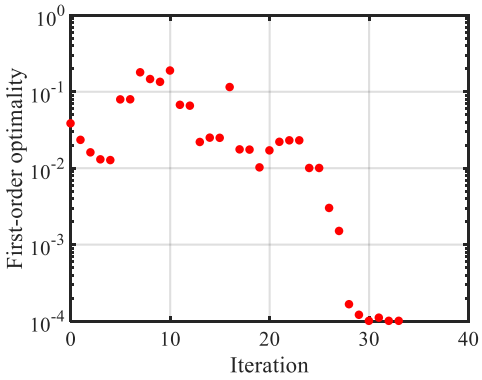

f) Fist order optimality (triggered transition)

Fig. 14 Optimization history

Table 13 Optimization results

Configuration	m_F, kg	MTOM, kg	m_{W+S}, kg	C_L	C_D	AR	Λ, deg
Reference A	16117	67262	11180	0.3893	0.0101	25.81	10.54
Optimized A	14406	61488	7735	0.3778	0.0047	26.01	8.88
Reference B	18722	70900	11262	0.4038	0.0101	25.81	10.54
Optimized B	17267	64707	7824	0.4042	0.0092	19.71	12.63

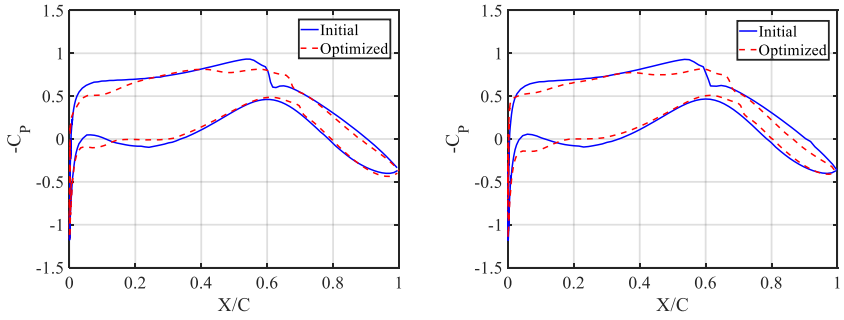

a) 0.00*b*

b) 0.25*b*

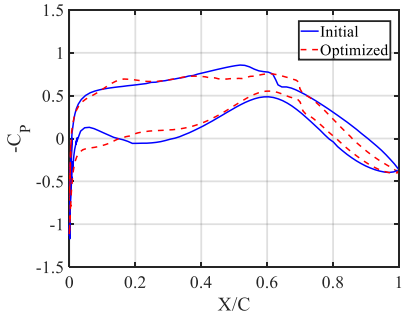

c) 0.50*b*

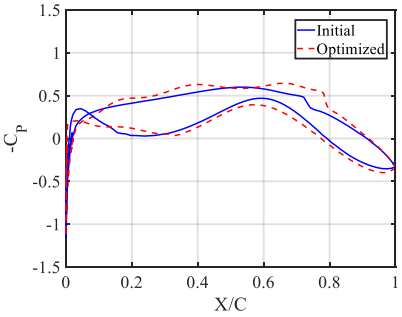

d) 0.75*b*

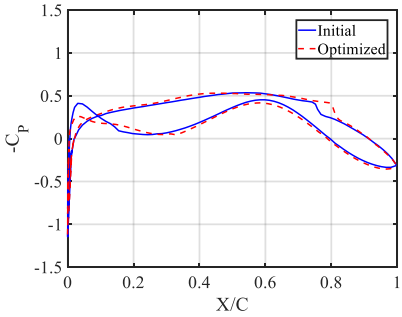

e) 1.00*b*

Fig. 15 Pressure distribution on sections perpendicular to the sweep line in different wing spanwise positions (free transition mode)

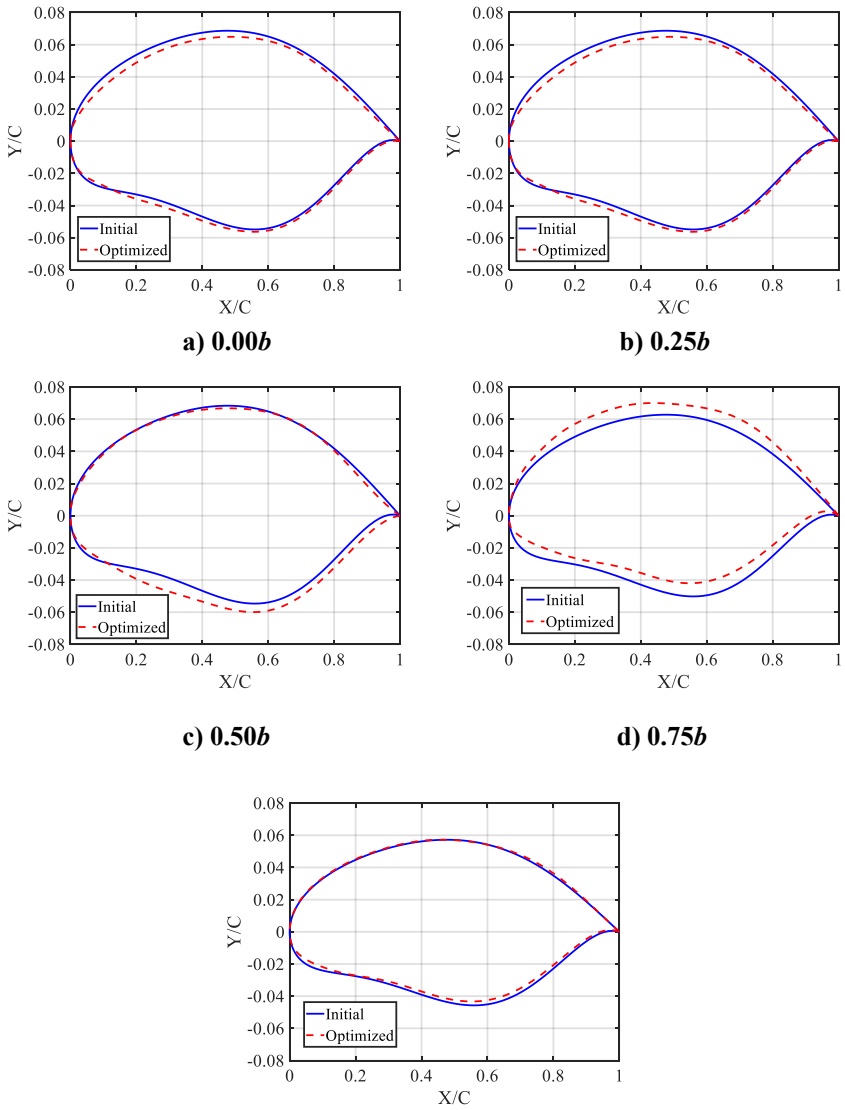

a) 0.00*b* **b) 0.25*b***

c) 0.50*b* **d) 0.75*b***

e) 1.00*b*

Fig. 16 Airfoil shape of the sections perpendicular to the sweep line in different wing spanwise positions (free transition mode)

Table 14 Drag coefficients

Configuration	C_D	C_{D_i}	C_{D_f}	C_{D_p}
Reference A	0.0068	0.0021	0.0035	0.0013
Optimized A	0.0047	0.0017	0.0023	6.77e-4
Reference B	0.0101	0.0021	0.0052	0.0028
Optimized B	0.0092	0.0024	0.0051	0.0017

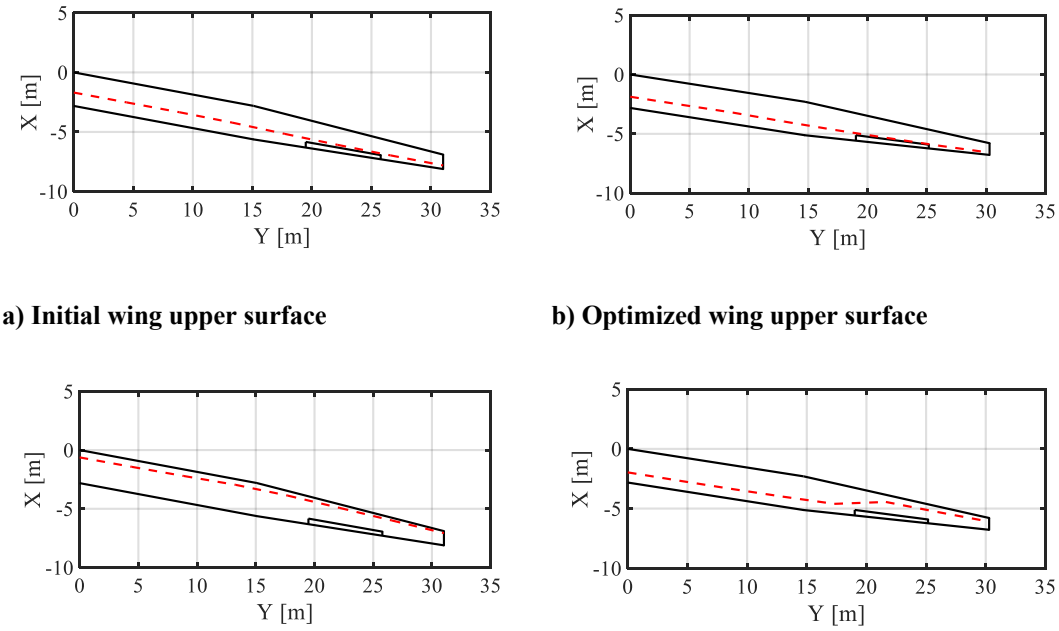

a) Initial wing upper surface

b) Optimized wing upper surface

c) Initial wing lower surface

d) Optimized wing lower surface

Fig. 17 Boundary layer transition profiles

As given in Table 13, the triggered transition mode optimization (Optimized B) reduced the fuel mass and aircraft MTOM by 7.77% and 8.73%, respectively. As shown in Fig. 18, the triggered transition mode optimization reduced the wing *AR* and increased the wing sweep angle to reduce the structural weight and total drag, especially the wave drag (see Fig. 19 and Fig. 20), thereby reducing the aircraft fuel mass.

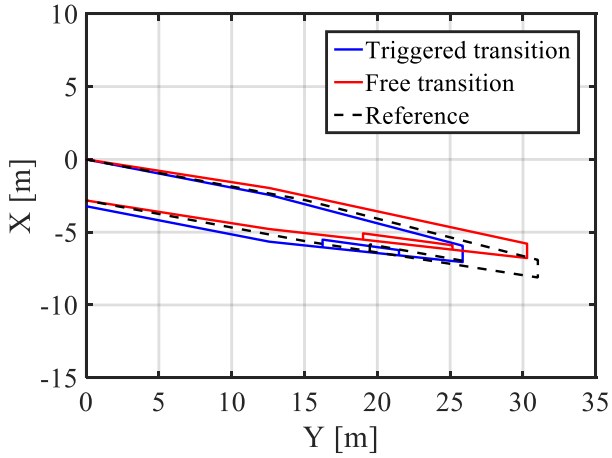

Fig. 18 Wing planform comparison

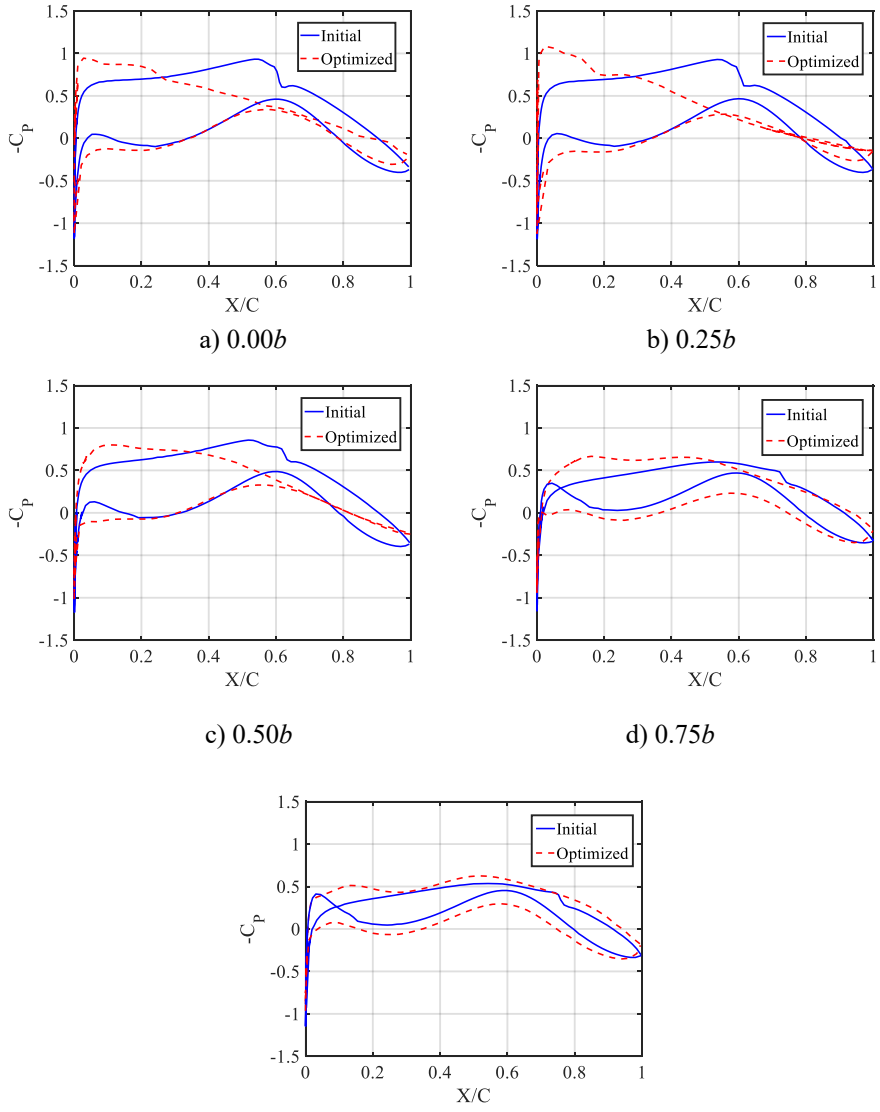

a) 0.00*b*

b) 0.25*b*

c) 0.50*b*

d) 0.75*b*

e) 1.00*b*

Fig. 19 Pressure distribution on sections perpendicular to the sweep line in different wing spanwise positions (triggered transition mode)

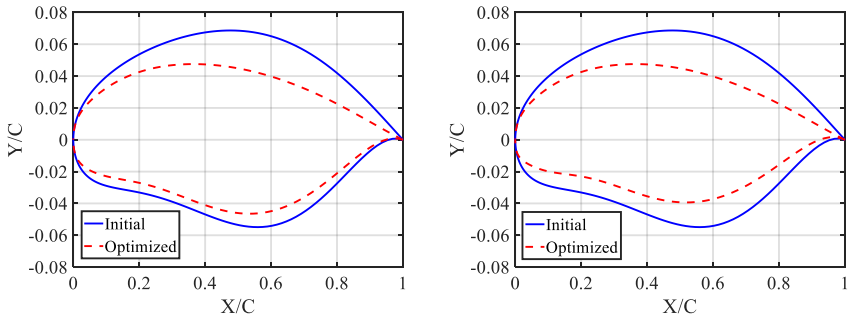

a) 0.00*b*

b) 0.25*b*

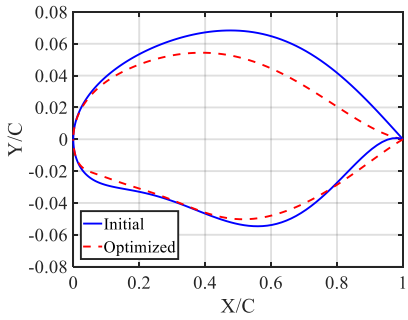

c) 0.50*b*

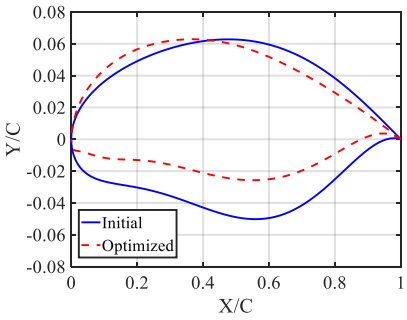

d) 0.75*b*

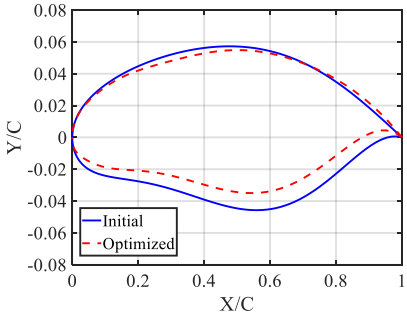

e) 1.00*b*

Fig. 20 Airfoil shape of the sections perpendicular to the sweep line in different wing spanwise positions (triggered transition mode)

In the free transition mode optimization, the optimizer tried to decrease the induced drag by increasing the wing *AR* and reducing the taper ratio to push the load distribution on the wing toward the elliptical lift distribution. However, from a structural point of view, those changes will increase the wing's structural weight. Therefore, at the same time, the optimizer reduced the wing sweep angle and made the optimized wing more flexible (see Fig. 21 and Fig. 22), resulting in a remarkable reduction in wing structural weight. This increased flexibility is achieved by reducing the thickness of the equivalent panels

and spars, especially for the outboard wing sections, as shown in Fig. 23. As a result, although the optimized wing's *AR* in free transition mode is 32% higher than that in triggered transition mode, their wing and strut structural weight are similar, as given in Table 13. It should be mentioned that the MR-SBW aircraft conceptual design took into account that the SBW concept could adopt thinner airfoils than the conventional cantilever wing aircraft. In both aerostructural optimizations presented in this section, the optimizer did not increase the wing thickness, i.e., the final optimized SBW is thinner than the cantilever wings of conventional aircraft. Besides, there are two constraints that prevent the optimizer from further reducing the wing thickness in the aerostructural optimization, i.e., available fuel volume and wing structural stiffness.

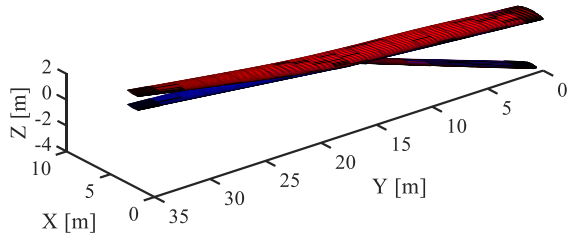

a) Initial wing under +1.5g

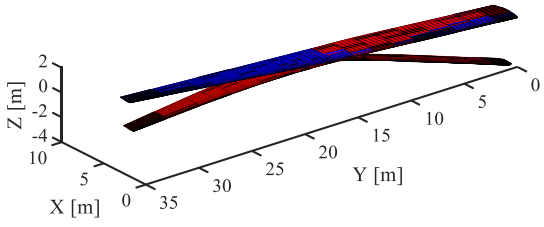

b) Initial wing under -0.5g

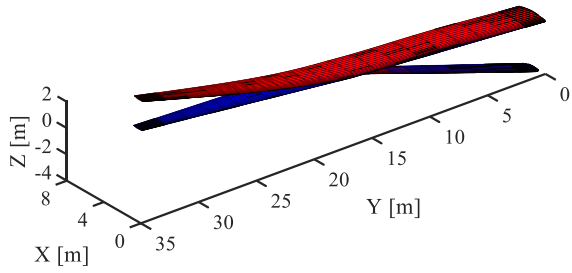

c) Optimized wing under +1.5g

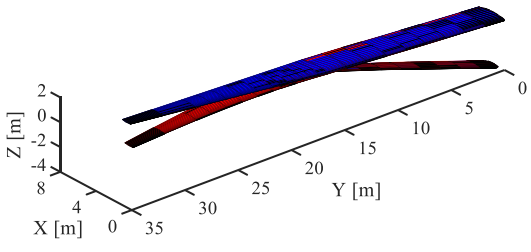

d) Optimized wing under -0.5g

Fig. 21 Wing deformed shaper and jig shape under maximum pull-up load

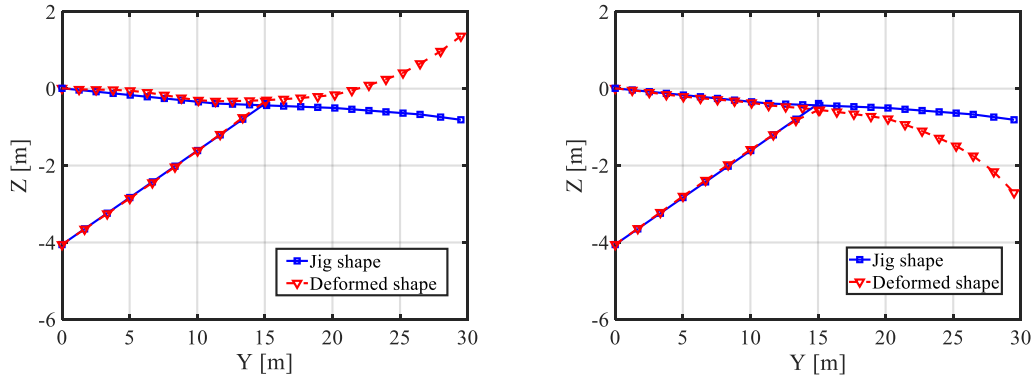

a) Max. positive load **b) Max. negative load**

Fig. 22 Wing deflection and the comparison between jig shape and deformed shape

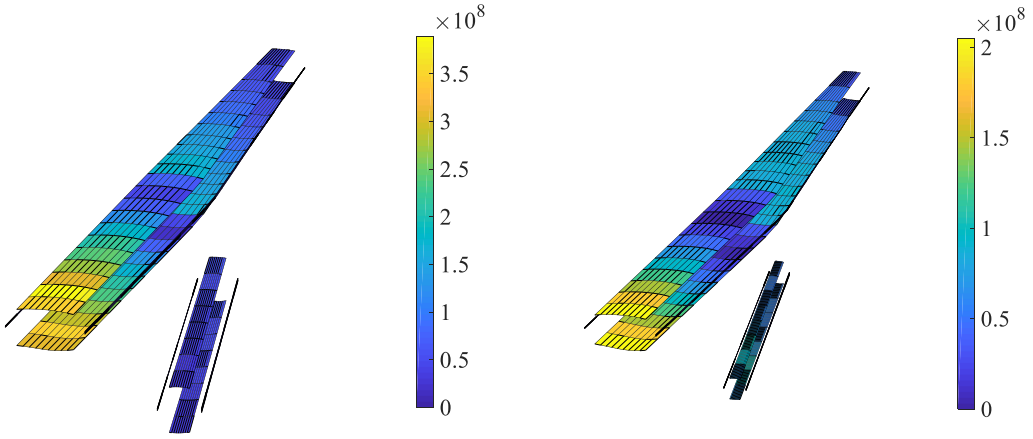

a) Initial (1.5g pull-up) b) Optimized (1.5g pull-up)

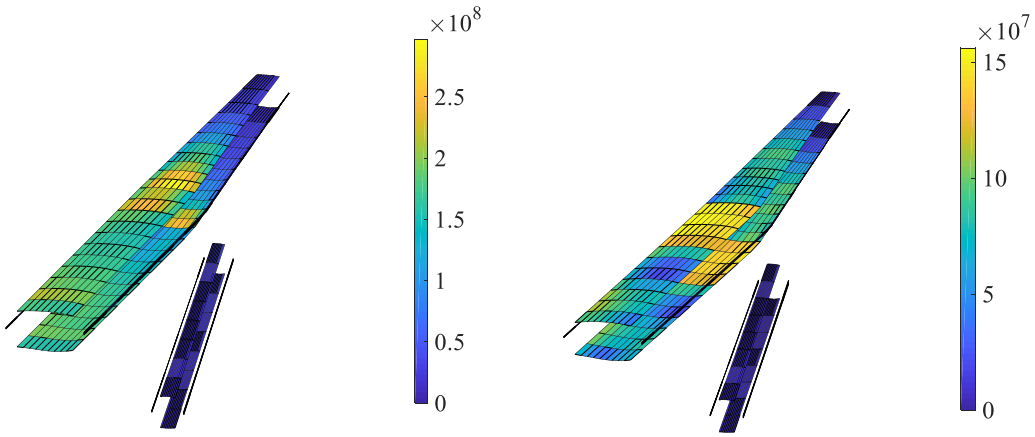

c) Initial (-0.5g push down) d) Optimized (-0.5g push down)

Fig. 23 Wing box von Mises stress distribution

An important factor affecting the wing structural mass is the aileron effectiveness, which is generally an active constraint and the wing mass increases quadratically with it [34]. As listed in Table 15, the optimized wing in free transition mode (Optimized A) has a larger *AR* that resulted in a larger aileron area and a larger aileron arm than that in triggered transition mode (Optimized B). Therefore, the same amount of L_δ was achieved with lower aileron effectiveness, i.e., 0.455 in free transition mode versus 0.502 in triggered transition mode. The wing mass breakdown comparison of the initial configuration, triggered transition mode optimized configuration, and free transition mode optimized configuration are given in Table 15. The wing mass of the reference configuration is significantly higher than that of the aerostructurally optimized one, even though the aileron effectiveness of the reference configuration is slightly less. The wing mass of the triggered transition mode optimization is lighter than that of the reference configuration mainly because its *AR* is significantly smaller (19.71 vs. 25.81), which is more significant than the influence of aileron effectiveness. The difference in wing mass between the free transition mode optimized configuration and the reference is due to the following reasons: 1) the MTOM of the optimized aircraft is smaller, so the wing mass will also be smaller; 2) the wing sweep angle of the optimized SBW is smaller, which can reduce the wing structural mass; 3) the wing stiffness is improved by adjusting the wing airfoil shapes and strut airfoil thickness-to-chord ratios in the aerostructural optimization. For comparison and reference purposes, the wing mass data of SUGAR aircraft [12] that features a truss-braced wing configuration and a similar wing *AR* are also presented. It can be seen that the wing structural mass accounts for about 80% of the total structural mass (total refers to wing plus strut) and the strut structural mass accounts for about 20% of the total structural mass.

Table 15 Wing mass breakdown and aileron effectiveness

Configuration	m_{W+S}, kg	m_W, kg	m_S, kg	m_W / m_{W+S}	m_S / m_{W+S}	η_α
Reference A	11418	8824.8	2593.2	0.77	0.23	0.381
Optimized A	7734.5	6072.6	1661.9	0.79	0.21	0.455
Reference B	11262	9158.8	2103.2	0.81	0.19	0.366
Optimized B	7823.8	6301.1	1522.7	0.81	0.19	0.502
SUGAR [12]	7561.4	5894.2	1667.2	0.78	0.22	--

For more comprehensive comparison and reference, a set of aerostructural optimizations were performed under conventional load conditions (i.e., +2.5 g/-1.0 g) and compared with the SUGAR aircraft, as given in Table 16. The Baseline free and Baseline triggered in Table 16 are baseline configurations for aerostructural optimization, resized for the same mission profile and the same top-level requirements under conventional load conditions at the conceptual design phase. The baseline configuration of the NLF design is significantly better than that of the conventional design, mainly due to the reduced drag of NLF technology. It is worth mentioning that the fuel weight and MTOM of the aerostructurally optimized MR-SBW aircraft in free transition mode are close to those of the SUGAR aircraft; while those of the triggered transition mode optimized MR-SBW aircraft are notably worse than free transition mode case and the SUGAR aircraft because of its worse starting point as well as the higher drag. The SUAGR aircraft employs the NLF wing design and thus performs much better than the "Optimized triggered" configuration. In addition, the SUGAR aircraft applies airframe structural weight reduction assumptions and fuselage riblets that were not considered in the MR-SBW aircraft presented in this paper. These advanced technologies and the associated snowball effect have also improved the SUGAR aircraft's performance.

Table 16 Comparison of the MR-SBW aircraft and the SUGAR aircraft (both under +2.5 g/-1.0 g load cases)

Configuration	Usable fuel, kg	MTOM, kg	m_{W+S} , kg	AR
Baseline free	16523	72334	12422	25.81
Optimized free	14540	67340	10510	23.33
Baseline triggered	22205	79944	14418	25.81
Optimized triggered	20128	76977	12526	17.70
SUGAR	14470	68039	9231	19.55

IV. Conclusion

This paper addressed the coupled adjoint aerostructural optimization of SBW aircraft configuration with ultra-high aspect ratio wings. Several methods and tools, including a mid-fidelity aerostructural optimization tool, were used and integrated into a framework for SBW aircraft conceptual design and optimization. A medium-range SBW aircraft was initially designed and optimized in the conceptual design stage and a secondary aerostructural optimization was performed for the SBW aircraft with the objective of fuel mass.

PyInit and SUAVE were employed for the initial sizing, performance analysis, and conceptual optimization of the MR-SBW aircraft. According to the previous uncertainty analysis results, an MR-SBW aircraft was initially designed with a Mach number of 0.735. The iterative aircraft performance assessment tool SUAVE was used for the conceptual optimization of the MR-SBW aircraft in terms of fuel mass. The optimization resulted in a 3.17% reduction in fuel mass.

A coupled adjoint aerostructural analysis and optimization tool FEMWET was presented and modified for the ultra-high aspect ratio SBW configuration and geometrically nonlinear composite

structures. The Q3D aerodynamic solver was utilized for NLF wing calculations. The proposed FEMWET tool was employed for the wing aerostructural optimization of the MR-SBW aircraft. The wing box structure, wing planform, wing airfoil shapes, and strut airfoil thickness-to-chord ratios were used as design variables. The optimization objective was to minimize the aircraft mission fuel mass while satisfying the constraints on the wing and strut structural failure, wing loading, and aileron effectiveness. The optimization results showed more than a 10% reduction in fuel mass, more than 8% reduction in aircraft MTOM, and more than 30% reduction in wing and strut structural mass. It should be mentioned that the aeroelastically optimized SBW is notably heavier than the conceptual design results due to the consideration of the aileron effectiveness constraint, which provides a worse starting point for the subsequent aerostructural optimization. As a result, this leads to a final aerostructurally optimized wing mass that is close to the conceptual design results, even though the aerostructural optimization has significantly reduced the wing mass.

This work studied preliminarily the aerostructural optimization for the SBW aircraft configuration. Avenues for future work include modeling flutter constraints and aileron sizing for UHARW configurations. Furthermore, this study focused on the SBW configuration, while future research will perform aeroelastic and aerostructural optimization for other promising UHARW configurations, e.g., the twin-fuselage configuration.

Funding Sources

This project has received partial funding from the Clean Sky 2 Joint Undertaking (JU) under grant agreement No 883670. The JU receives support from the European Union's Horizon 2020 research and innovation programme and the Clean Sky 2 JU members other than the Union.

Acknowledgments

The authors would like to thank Anand Sudhi, Camli Badrya and Rolf Radespiel for sharing the initial NLF airfoil geometry.

References

[1]. Boeing, Commercial Market Outlook 2019-2038. 2019.

[2]. Airbus, Global Market Forecast 2018-2037, Global Networks, Global Citizens, ISBN: 978-2-9554382-3-6, 2018.

[3]. Eisenhut, D., Moebs, N., Windels, E., Bergmann, D., Geiß, I., Reis, R., and Strohmayer, A., "Aircraft Requirements for Sustainable Regional Aviation," *Aerospace*, 2021. 8(3): p. 61. https://doi.org/10.3390/aerospace8030061

[4]. Greitzer, E. M., Bonnefoy, P. A., de la Rosa Blanco, E., Dorbian, C. S., Drela, M., Hall, D. K., Hansman, R. J., Hileman, J. I., Liebeck, R. H., Lovergren, J.,Mody, P., Pertuze, J. A., Sato, S., Spakovsky, Z. S., Tan, C. S., Hollman, J. S., Duda, J. E., Fitzgerald, N., Houghton, J., Kerrebrock, J. L., Kiwada, G. F., Kordonowy, D., Parrish, J. C., Tylko, J., Wen, E. A., and Lord, W. K., "N+3 Aircraft Concept Designs and Trade Studies Final Report," NASA CR-2010-216794/VOL2, 2010.

[5]. *Flightpath 2050-Europe's Vision for Aviation: Advisory Council for Aeronautics Research in Europe*, EUROPEAN COMMISSION: Brussels, Belgium, 2011.

[6]. Grewe, V., Rao, A. G., Grönstedt, T., Xisto, C., Linke, Florian., Melkert, J., Middel, J., Ohlenforst, B., Blakey, S., Christie, S., Matthes, S., and Dahlmann, K., "Evaluating the Climate Impact of Aviation Emission Scenarios Towards the Paris Agreement including COVID-19 Effects," *Nature Communications*, Vol. 12, No. 1, 2021, pp. 1-10. https://doi.org/10.1038/s41467-021-24091-y

[7]. Karpuk, S., and Elham, A., "Conceptual Design Trade Study for an Energy-Efficient Mid-Range Aircraft with Novel Technologies," AIAA paper 2021-0013, Jan. 2021. https://doi.org/10.2514/6.2021-0013

[8]. Chau, T. and D.W. Zingg, "Aerodynamic Optimization of a Transonic Strut-Braced-Wing Regional Aircraft Based on the Reynolds-Averaged Navier-Stokes Equations," AIAA paper 2021-2526, 2021. https://doi.org/10.2514/6.2021-2526

[9]. Reddy, J.N., *Mechanics of laminated composite plates and shells*. 2004: New York: CRC Press.

[10]. Gur, O., J.A. Schetz and W.H. Mason, "Aerodynamic Considerations in the Design of Truss-Braced-Wing Aircraft," *Journal of Aircraft*, 2011. 48(3): p. 919-939. https://doi.org/ 10.2514/1.C031171

[11]. Shirley, C. M., Schetz, J. A., Kapania, R. K., and Haftka, R. T. "Tradeoffs of Wing Weight and Lift/Drag in Design of Medium-Range Transport Aircraft," *Journal of Aircraft*, 51(3), 904-912. https://doi.org/10.2514/1.C032605

[12]. Bradley, M. K., Droney, C. K., and Allen, T. J., "Subsonic Ultra Green Aircraft Research: Phase II – Volume I – Truss Braced Wing Design Exploration," NASA/CR–2015-218704/Volume I, 2015.

[13]. Khan, K. H., Mallik, W., Kapania, R. K., and Schetz, J. A., "Distributed Design Optimization of Large Aspect Ratio Wing Aircraft with Rapid Transonic Flutter Analysis in Linux," AIAA Paper 2021-1354, Jan. 2021.

https://doi.org/10.2514/6.2021-1354

[14]. Carrier, G.G., Arnoult, G., Fabbiane, N., Schotte, J., David, C., Defoort, S., Benard, E., and Delavenne, M., "Multidisciplinary analysis and design of strut-braced wing concept for medium range aircraft," AIAA paper 2022-0726, Jan. 2022.
https://doi.org/10.2514/6.2022-0726

[15]. Xiong, J., N. Nguyen, and R.E. Bartels, "Aeroelastic Analysis of Mach 0.8 Transonic Truss-Braced Wing Aircraft," AIAA paper 2022-0300, Jan. 2022.
https://doi.org/10.2514/6.2022-0300

[16]. Xiong, J., N. Nguyen, and R.E. Bartels, "Aerodynamic Optimization of Mach 0.8 Transonic Truss-Braced Wing Aircraft using Variable Camber Continuous Trailing Edge Flap," AIAA paper 2022-0016, Jan. 2022.
https://doi.org/10.2514/6.2022-0016

[17]. Secco N. R, and Martins J. R. R. A., "RANS-based aerodynamic shape optimization of a strut-braced wing with overset meshes," *Journal of Aircraft*, 2019, 56(1): 217-227.
https://doi.org/10.2514/1.C034934

[18]. Meadows, N. A., Schetz, J. A., Kapania, R. K., Bhatia, M., & Seber, G., "Multidisciplinary Design Optimization of Medium-Range Transonic Truss-Braced Wing Transport Aircraft," *Journal of Aircraft*, 2012. 49(6): p. 1844-1856.
https://doi.org/10.2514/1.C031695

[19]. Gur, O., Bhatia, M., Schetz, J. A., Mason, W. H., Kapania, R. K., and Mavris, D. N. "Design optimization of a truss-braced-wing transonic transport aircraft," *Journal of aircraft*, 47(6), 2010, 1907-1917.
https://doi.org/10.2514/1.47546

[20]. Kassapoglou, C., *Design and analysis of composite structures: with applications to aerospace structures*, John Wiley & Sons, 2013.

[21]. Gray, A.C. and J.R.R.A. Martins, "Geometrically Nonlinear High-fidelity Aerostructural Optimization for Highly Flexible Wings," AIAA paper 2021-0283, Jan. 2021.
https://doi.org/10.2514/6.2021-0283

[22]. Riso, C., Di Vincenzo, F. G., Ritter, M., Cesnik, C. E., and Mastroddi, F., "Nonlinear aeroelastic trim of very flexible aircraft described by detailed models," *Journal of Aircraft*, 55(6), 2018, pp. 2338-2346.
https://doi.org/10.2514/1.C034787

[23]. Castellani M, Cooper J E, and Lemmens Y. "Nonlinear static aeroelasticity of high-aspect-ratio-wing aircraft by finite element and multibody methods," *Journal of Aircraft*, 2017, 54(2): pp. 548-560.
https://doi.org/10.2514/1.C033825

[24]. Werter, N. P. M., and De Breuker, R., "A novel dynamic aeroelastic framework for aeroelastic tailoring and structural optimization," *Composite Structures*, 2016, 158, 369-386.
https://doi.org/10.1016/j.compstruct.2016.09.044

[25]. Conlan-Smith, C., and Andreasen, C. S., "Aeroelastic shape optimization of solid foam core wings subject to large deformations," *Structural and Multidisciplinary Optimization*, 2022, 65(6), 1-18.
https://doi.org/10.1007/s00158-022-03246-5

[26]. Achard, T., Blondeau, C., and Ohayon, R., "High-Fidelity Aerostructural Gradient Computation Techniques with Application to a Realistic Wing Sizing," *AIAA Journal*, 2018, 56(11), 4487-4499.

https://doi.org/10.2514/1.J056736

[27]. McDonald, R. A., German, B. J., Takahashi, T., Bil, C., Anemaat, W., Chaput, A., Vos, R., and Harrison, N., "Future aircraft concepts and design methods," *The Aeronautical Journal*, 2022, 126(1295), 92-124.
https://doi.org/10.1017/aer.2021.110

[28]. Sohst, M., do Vale, J. L., Afonso, F., and Suleman, A., "Optimization and comparison of strut-braced and high aspect ratio wing aircraft configurations including flutter analysis with geometric non-linearities," *Aerospace Science and Technology*, 2022, 124, 107531.
https://doi.org/10.1016/j.ast.2022.107531

[29]. Yang, T., Chen, Y., Shi, Y., Hua, J., Qin, F., and Bai, J., "Stochastic Investigation on the Robustness of Laminar-Flow Wings for Flight Tests," *AIAA Journal*, 2022, 60(4), 2266-2286.
https://doi.org/10.2514/1.J060842

[30]. Xu, J., and Kroo, I., "Aircraft design with active load alleviation and natural laminar flow," *Journal of Aircraft*, 2014, 51(5), 1532-1545.
https://doi.org/10.2514/1.C032402

[31]. Schrauf, G., "Status and perspectives of laminar flow," *The aeronautical journal*, 2005, 109(1102), 639-644.
https://doi.org/10.1017/S000192400000097X

[32]. Kruse, M., Wunderlich, T., and Heinrich, L., "A conceptual study of a transonic NLF transport aircraft with forward swept wings," AIAA paper 2012-3208, Sept. 2012.
https://doi.org/10.2514/6.2012-3208

[33]. Han, Z. H., Chen, J., Zhang, K. S., Xu, Z. M., Zhu, Z., and Song, W. P., "Aerodynamic shape optimization of natural-laminar-flow wing using surrogate-based approach," *AIAA Journal*, 2018, 56(7), 2579-2593.
https://doi.org/10.2514/1.J056661

[34]. Elham, A. and M.J. van Tooren, "Tool for preliminary structural sizing, weight estimation, and aeroelastic optimization of lifting surfaces," *Proceedings of the Institution of Mechanical Engineers, Part G: Journal of Aerospace Engineering*, 2015. 230(2): p. 280-295.
https://doi.org/10.1177/0954410015591045

[35]. Riso, C., Sanghi, D., Cesnik, C. E., Vetrano, F., and Teufel, P., "Parametric roll maneuverability analysis of a high-aspect-ratio-wing civil transport aircraft," In AIAA paper 2020-1191, Jan. 2020.
https://doi.org/10.2514/6.2020-1191

[36]. Sanghi, D., Riso, C., Cesnik, C., and Vetrano, F., "Influence of Aileron Placement on Roll Response of High-Aspect-Ratio-Wing Aircraft," In AIAA paper 2020-2645, June 2020.
https://doi.org/10.2514/6.2020-2645

[37]. Boozer, C. M, and Elham, A., "Coupled-adjoint aerostructural optimisation framework for aircraft preliminary design," ICAS 2018, 10-14 September, Belo Horizonte, Brazil

[38]. Guo, J., Li, Y., Xu, M., An, X., and Li, G., "Aero-structural optimization of supersonic wing under thermal environment using adjoint-based optimization algorithm," *Structural and Multidisciplinary Optimization*, 2021, 64(1), 281-301.
https://doi.org/10.1007/s00158-021-02888-1

[39]. Martins, J. R., Kennedy, G., and Kenway, G. K., "High aspect ratio wing design: Optimal aerostructural tradeoffs for the next generation of materials," AIAA paper 2014-0596, Jan. 2014.
https://doi.org/10.2514/6.2014-0596

[40]. Brooks, T. R., Martins, J. R., and Kennedy, G. J., "High-fidelity aerostructural optimization of tow-steered composite wings," *Journal of Fluids and Structures*, 2019, 88, 122-147. https://doi.org/10.1016/j.jfluidstructs.2019.04.005

[41]. Ma, Y., S. Karpuk and A. Elham, "Conceptual design and comparative study of strut-braced wing and twin-fuselage aircraft configurations with ultra-high aspect ratio wings," *Aerospace Science and Technology*, 2022: p. 107395. https://doi.org/10.1016/j.ast.2022.107395

[42]. Lukaczyk, T. W., Wendorff, A. D., Colonno, M., Economon, T. D., Alonso, J. J., Orra, T. H., and Ilario, C., "SUAVE: an Open-Source Environment for Multi-Fidelity Conceptual Vehicle Design," AIAA Paper 2015-3087, June 2015. https://doi.org/10.2514/6.2015-3087

[43]. Elham, A. and M.J.L. van Tooren, "Coupled adjoint aerostructural wing optimization using quasi-three-dimensional aerodynamic analysis," *Structural and Multidisciplinary Optimization*, 2016. 54(4): p. 889-906. https://doi.org/10.1007/s00158-016-1447-9

[44]. Botero, E M., Wendorff, A., MacDonald, T., Variyar, Anil., Vegh, J. M., Lukaczyk, T. e., Alonso, J., Orra, T., and da Silva, C., "Suave: An open-source environment for conceptual vehicle design and optimization," *54th AIAA Aerospace Sciences Meeting*. 2016: 1275. https://doi.org/10.2514/6.2016-1275

[45]. Jones, E., Oliphant, T., and Peterson, P., SciPy: Open source scientific tools for Python. 2001.

[46]. Harrison, N. A., Gatlin, G. M., Viken, S. A., Beyar, M., Dickey, E. D., Hoffman, K., and Reichenbach, E. Y., "Development of an Efficient M= 0.80 Transonic Truss-Braced Wing Aircraft," AIAA Paper 2020-0011, Jan. 2020. https://doi.org/10.2514/6.2020-0011

[47]. Abouhamzeh M, Ma Y, and Elham A. "A Geometrically Nonlinear Structural Model For Aerostructural Optimization of Ultra-High Aspect Ratio Composite Wings," *AIAA SCITECH 2022 Forum*. 2022: 0724. https://doi.org/10.2514/6.2022-0724.vid

[48]. Vo, T. P., and Lee, J., "Geometrically nonlinear analysis of thin-walled composite box beams," *Computers & Structures*, 2009, 87(3-4), 236-245. https://doi.org/10.1016/j.compstruc.2008.10.002

[49]. Cestino, E., and Frulla, G., "Analysis of slender thin-walled anisotropic box-beams including local stiffness and coupling effects," *Aircraft Engineering and Aerospace Technology*, 2014, Vol. 86 No. 4, pp. 345-355. https://doi.org/10.1108/AEAT-10-2012-0159

[50]. Librescu, L., and O. Song, *Thin Walled Composite Beams: Theory and Applications,* 2006, Dordrecht, the Netherlands: Springer.

[51]. Minguet, P., and Dugundji, J., "Experiments and analysis for composite blades under large deflections. I-Static behavior," *AIAA journal*, 1990, 28(9), 1573-1579. https://doi.org/10.2514/3.25255

[52]. Cesnik, C. E., and Hodges, D. H., "VABS: a new concept for composite rotor blade cross‐sectional modeling," *Journal of the American helicopter society*, 1997, 42(1), 27-38. *https://doi.org/10.4050/JAHS.42.27*

[53]. Elham, A., "Adjoint quasi-three-dimensional aerodynamic solver for multi-fidelity wing

aerodynamic shape optimization," *Aerospace Science and Technology*, 2015. 41: p. 241-249. https://doi.org/10.1016/j.ast.2014.12.024

[54]. Drela, M., MSES: Multi-Element Airfoil Design/Analysis Software. Ver. 3.07, Massachusetts Institute of Technology, 2007.

[55]. Drela M., "Design and optimization method for multi-element airfoils," *Aerospace Design Conference*. 1993: 969. https://doi.org/10.2514/6.1993-969

[56]. P Chiozzotto, G., "Wing weight estimation in conceptual design: a method for strut-braced wings considering static aeroelastic effects," CEAS Aeronautical Journal, 2016, 7(3), 499-519. https://doi.org/10.1007/s13272-016-0204-5

[57]. Rump S M., "INTLAB—interval laboratory," *Developments in reliable computing*. Springer, Dordrecht, 1999: 77-104. https://doi.org/10.1007/978-94-017-1247-7_7

[58]. Roskam., J., *Airplane design, Part, I: Preliminary sizing of airplanes*. 1986, Lawrence Kansas: DAR corporation.

[59]. Vo, T. P., and Lee, J., "Geometrically nonlinear theory of thin-walled composite box beams using shear-deformable beam theory," *International journal of mechanical sciences*, 2010, 52(1), 65-74. https://doi.org/10.1016/j.ijmecsci.2009.10.005

[60]. Elham, A. and M.J.L. van Tooren, "Effect of wing-box structure on the optimum wing outer shape," *Aeronautical journal*, 2014. 118(1199): p. 1-30. https://doi.org/10.1017/S0001924000008903

[61]. Ma, Y., Minisci, E., and Elham, A., "Investigating the Influence of Uncertainty in Novel Airframe Technologies on Realizing Ultra-high Aspect Ratio Wings", in AeroBest 2021. 2021.

[62]. Wunderlich, T. F., Dähne, S., Reimer, L., and Schuster, A., "Global aero-structural design optimization of composite wings with active maneuver load alleviation," CEAS Aeronautical Journal, 2022, 13, 639–662. https://doi.org/10.1007/s13272-022-00585-3

[63]. Chiozzotto, G.P., "Initial weight estimate of advanced transport aircraft concepts considering aeroelastic effects," AIAA Paper 2017-0009, Jan. 2017. https://doi.org/10.2514/6.2017-0009

[64]. Gur, O., Bhatia, M., Mason, W. H., Schetz, J. A., Kapania, R. K., and Nam, T., "Development of a framework for truss-braced wing conceptual MDO," *Structural and Multidisciplinary optimization*, 2011, 44(2), 277-298. https://doi.org/10.1007/s00158-010-0612-9

[65]. Shevell, R. S., *Fundamentals of flight*, 1989, Pearson Education India.

[66]. Metkowski L P, and Maughmer M. "Winglet and Strut Configuration Study for a Slotted, Natural-Laminar-Flow Strut-Braced Transport Aircraft," *AIAA Scitech 2021 Forum*. 2021: 0843. https://doi.org/10.2514/6.2021-0843

[67]. Adler, E., and Martins, J. R., "Aerostructural wing design optimization considering full mission analysis," AIAA paper 2022-0382, Dec. 2021. https://doi.org/10.2514/6.2022-0382

[68]. Sadraey, M.H., *Aircraft design: A systems engineering approach*. 2012: John Wiley & Sons.

[69]. Roskam, J., *Airplane Design Part V: Component Weight Estimation*. 1985: DAR corporation.

[70]. Sudhi A, Radespiel R, and Badrya C. "Design of Transonic Swept Wing for HLFC Application,"

AIAA Aviation 2021 Forum. 2021: 2606.
https://doi.org/10.2514/6.2021-2606